New Phytologist

Research

A transcription factor of the NAC family regulates nitrate-induced legume nodule senescence

Longlong Wang[1], Tao Tian[1], Jianjun Liang[1], Runhui Li[2], Xian Xin[3], Yongmei Qi[1], Yumiao Zhou[1], Qiuling Fan[1], Guogui Ning[2], Manuel Becana[4] and Deqiang Duanmu[1]

[1]State Key Laboratory of Agricultural Microbiology, Hubei Hongshan Laboratory, Huazhong Agricultural University, Wuhan 430070, China; [2]National Key Laboratory for Germplasm Innovation & Utilization of Horticultural Crops, Huazhong Agricultural University, Wuhan 430070, China; [3]Biotech Research and Innovation Centre, Faculty of Health and Medical Sciences, University of Copenhagen, DK-2200 Copenhagen, Denmark; [4]Departamento de Biología Vegetal, Estación Experimental de Aula Dei, Consejo Superior de Investigaciones Científicas, Avenida Montañana 1005, 50059 Zaragoza, Spain

Author for correspondence:
Deqiang Duanmu
Email: duanmu@mail.hzau.edu.cn

Received: *10 January 2023*
Accepted: *12 March 2023*

New Phytologist (2023) **238:** 2113–2129
doi: 10.1111/nph.18896

Key words: legume nodules, *Lotus japonicus*, NAC transcription factor, nitrate, nodule senescence, senescence-associated genes (*SAGs*).

Summary

- Legumes establish symbioses with rhizobia by forming nitrogen-fixing nodules. Nitrate is a major environmental factor that affects symbiotic functioning. However, the molecular mechanism of nitrate-induced nodule senescence is poorly understood.
- Comparative transcriptomic analysis reveals an NAC-type transcription factor in *Lotus japonicus*, LjNAC094, that acts as a positive regulator in nitrate-induced nodule senescence. Stable overexpression and mutant lines of *NAC094* were constructed and used for phenotypic characterization. DNA-affinity purification sequencing was performed to identify NAC094 targeting genes and results were confirmed by electrophoretic mobility shift and transactivation assays.
- Overexpression of *NAC094* induces premature nodule senescence. Knocking out *NAC094* partially relieves nitrate-induced degradation of leghemoglobins and abolishes nodule expression of senescence-associated genes (*SAGs*) that contain a conserved binding motif for NAC094. Nitrate-triggered metabolic changes in wild-type nodules are largely affected in *nac094* mutant nodules. Induction of *NAC094* and its targeting *SAGs* was almost blocked in the nitrate-insensitive *nlp1*, *nlp4*, and *nlp1 nlp4* mutants.
- We conclude that NAC094 functions downstream of NLP1 and NLP4 by regulating nitrate-induced expression of *SAGs*. Our study fills in a key gap between nitrate and the execution of nodule senescence, and provides a potential strategy to improve nitrogen fixation and stress tolerance of legumes.

Introduction

Nitrogen is an indispensable nutrient for all living organisms as it is a major constituent of amino acids, nucleotides, porphyrins, flavins, and other relevant metabolites. Plants acquire nitrogen from the soil in organic and inorganic forms. In particular, nitrate is widely present in agricultural and natural ecosystems (Vidal *et al.*, 2020). The application of nitrate-based fertilizers has dramatically enhanced crop yields since the first Green Revolution. However, the excessive use of fertilizers inevitably leads to environmental problems (Wang *et al.*, 2018). Significant progress has been made in elucidating genetic networks of nitrate signaling in plants (Vidal *et al.*, 2020). The NIN-LIKE PROTEIN (NLP) family of transcription factors (TFs) are master regulators in the nitrate signaling pathway (Liu *et al.*, 2017). The central roles of NLPs in controlling nitrate transport, sensing, and metabolism have been characterized in model and crop plants, including *Arabidopsis thaliana* (Konishi *et al.*, 2021; Liu *et al.*, 2022), rice (Wu *et al.*, 2020; Yu *et al.*, 2021), maize (Ge *et al.*, 2020), and legumes (Lin *et al.*, 2018; Nishida *et al.*, 2018; Jiang *et al.*, 2021). Understanding how NLPs are involved in the nitrate regulatory network is an important foundation to breed crops with improved nitrogen use efficiency and with reduced fertilizer demands.

Legumes can establish symbiotic interactions with rhizobia, which permit them to use atmospheric nitrogen (N_2) as the sole nitrogen source. As a result of a molecular dialogue between the rhizobia and the plants, new symbiotic organs, the nodules, are formed on the roots. In the nodules, rhizobia differentiate into bacteroids that express the nitrogenase enzyme complex, which reduces ('fixes') N_2 to ammonia. This symbiotic nitrogen fixation (SNF) is inhibited by excess nitrate at different stages, from rhizobial infection to nodule development and senescence (Nishida & Suzaki, 2018). Legumes have developed adaptive strategies to sense environmental nitrogen levels and to regulate SNF to reduce unnecessary consumption of sucrose derived from

photosynthesis. Several studies have uncovered the central roles of NLPs in nitrate-triggered inhibition of SNF. In the model legume *Lotus japonicus*, NLP4 controls the nodule number by directly regulating the expression of CLE-RS2, a root-derived mobile peptide that works as a negative regulator of nodule formation (Nishida *et al.*, 2018). Further studies show that *L. japonicus* NLP1 and NLP4 have overlapping functions in controlling nitrate inhibition of nodule development. NLP4 competes for binding sites on target genes with NIN (NODULE INCEPTION), an essential TF required for nodule organogenesis (Schauser *et al.*, 1998; Lin *et al.*, 2021; Nishida *et al.*, 2021). In addition, NLP1 regulates the expression of a nitrate transporter gene, *NRT2.1*, to mediate root nodule formation under low- and high-nitrate conditions (Misawa *et al.*, 2022; Luo *et al.*, 2023). These findings underpin a central role of NLPs in controlling nitrate responses at the early stages of SNF. The absence of both NLP1 and NLP4 virtually abolishes nitrate-triggered inhibition of SNF in mature nodules, suggesting an additional function of NLPs in controlling later stages of symbiosis (Nishida *et al.*, 2021). However, the question of how NLPs regulate nodule functioning or senescence remains unanswered.

Legume nodule senescence is a fine-tuned process that occurs at the late stage of development (nodule aging) or that is induced by adverse environmental factors (Loscos *et al.*, 2008; Dupont *et al.*, 2012). Premature nodule senescence was also observed in several plant mutants, such as *sen1* (Suganuma *et al.*, 2003) and leghemoglobin (Lb) triple mutant *lb123* (Wang *et al.*, 2019). Developmental and premature nodule senescence share some features, such as the inhibition of nitrogenase, activation of proteases, degradation of Lb, and alteration of redox homeostasis; however, the two types of senescence have also differential effects on nodule ultrastructure and functioning and on the expression of multiple genes and proteins (Minchin *et al.*, 1989; Gogorcena *et al.*, 1997; Puppo *et al.*, 2005; Van de Velde *et al.*, 2006; Pérez Guerra *et al.*, 2010; Dupont *et al.*, 2012). Transcriptomic studies uncovered multiple sets of nodule genes that are responsive to developmental senescence (Van de Velde *et al.*, 2006) or to senescence induced by nitrate (Cabeza *et al.*, 2014), darkness (Pérez Guerra *et al.*, 2010), nitric oxide (De Michele *et al.*, 2009), or drought (Sańko-Sawczenko *et al.*, 2019). So far, only a few TFs have been identified with potential functions in regulating nodule senescence. In *Medicago truncatula*, the expression of *NAC969* is regulated by salt and nitrate in roots and nodules, and the knockdown of this gene triggers premature nodule senescence (de Zélicourt *et al.*, 2012). Another TF of the same legume, bHLH2, inhibits the expression of a senescence-related cysteine protease gene (*CP77*) by directly binding to its promoter (Deng *et al.*, 2019). However, positive regulators and transcriptional networks that promote nodule senescence have not been discovered yet.

Here, we have performed a time-course transcriptomic study in nodules of *L. japonicus* exposed to nitrate and subsequent nitrate removal. Comparison of this study with other transcriptome data allowed us to identify a unique TF, termed NAC094, that acts as a positive regulator of nodule senescence. The important role of this TF was confirmed by the phenotypic characterization of plants that overexpress or lack NAC094 in nodules. Binding motifs and regulatory gene targets were further identified by DNA affinity purification sequencing (DAP-seq). Additional studies with mutants reveal that NAC094 operates downstream of NLP4 and NLP1 to specifically activate the expression of senescence-associated genes (*SAGs*), which are required for nitrate-induced nodule senescence. Taken together, our findings underscore the role of NAC094 as a positive regulator of nodule senescence in mediating nitrate signal and promoting senescence-associated processes.

Materials and Methods

Plant materials and growth conditions

Lotus japonicus ecotype MG-20 and *Mesorhizobium loti* MAFF303099 were used in all the nodulation experiments. The *nac094* knockout mutants were generated using CRISPR-Cas9 (Wang *et al.*, 2016) and the *NAC094-OE* lines by overexpressing the *NAC094* coding sequence under the control of the *L. japonicus Lb2* expression cassette (Wang *et al.*, 2019). The *nlp1* and *nlp4* single mutants and the *nlp1 nlp4* double mutant were previously described (Nishida *et al.*, 2018, 2021). To analyze the effect of nitrate on changes in the nodule transcriptome, plants with nodules at 4 wk post-inoculation (wpi) were watered with Broughton and Dilworth (B&D) solution supplemented with 10 mM KNO_3 for 6 d consecutively. Nitrate was then gradually removed by watering with nitrate-free B&D solution for 5 d. The nitrate response of *nlp* and *nac094* mutants was examined at the later stages of nodule development. Nodulated plants at 4 wpi were watered with B&D solution containing 10 mM KNO_3 for 7 d. Detailed information is described in Supporting Information Methods S1.

Plasmid constructs

The binary vector for *NAC094* knockout was constructed according to Wang *et al.* (2016). For the overexpression constructs, the coding sequences of NAC094 (375 residues) and $NLP4^C$ (544–976 residues) were cloned into the *Lb2* expression cassette (Wang *et al.*, 2019). To construct the promoter-GUS fusion constructs, the promoter regions of *NAC094*, *CYP1*, *LYS*, *PTR*, and *COPT* were cloned into a DX2181-GUS construct. The construct for the DAP-seq experiment was generated by cloning the coding sequence of *NAC094* in the pFN19K HaloTag T7 SP6 Flexi expression vector (Promega). For reporter constructs, multiple promoters with different lengths were cloned into the DX2181-LUC-REN vector. For subcellular localization studies, the coding sequence of *NAC094* was cloned into *pUbq1::sGFP* to generate *pUbq1::NAC094-sGFP*. Detailed information is described in Methods S1. All primers used in this study are listed in Table S1.

Plant transformation

The hairy root and stable transformations of *L. japonicus* MG-20 plants were performed following previously described procedures

(Díaz *et al.*, 2005; Tirichine *et al.*, 2005) with minor modifications. For hairy root transformation, *Agrobacterium rhizogenes* LBA1334 was used for the induction of transgenic hairy root. For stable transformation, *Agrobacterium tumefaciens* EHA105 was used for the induction of transgenic callus. After a series of tissue culture procedures, the transgenic plants were finally obtained. Detailed information is given in Methods S1.

GUS staining

Nodules were harvested and immersed in the staining buffer containing 100 mM potassium phosphate (pH 7.0), 1 mM potassium ferrocyanide, 1 mM potassium ferricyanide, 0.1% (w/v) sodium lauroyl sarcosinate, 10 mM EDTA, 0.1% (v/v) Triton X-100, and 0.5 mg ml^{-1} of 5-bromo-4-chloro-3-indolyl-β-D-glucuronic acid cyclohexylammonium salt (Sangon Biotech, Shanghai, China). The reaction was at room temperature under vacuum for 2 h and then at 37°C overnight. Nodules were sectioned using a vibratome (VT 1000S; Leica, Wetzlar, Germany). Images were captured with a light microscope (DM2500; Leica). Details are given in Methods S1.

Immunoblot analysis

Fresh nodules (150–200 mg) were collected and nodule protein was precipitated with chloroform/methanol (Zhang *et al.*, 2021). The protein pellet was dissolved in sample buffer (50 mM Tris–HCl, pH 6.8, 5% SDS) and protein concentration was determined using a BCA protein assay kit (Sangon Biotech). Immunoblot analysis was performed following a standard protocol (Zhang *et al.*, 2021). Detailed procedures and antibody information are described in Methods S1.

Acetylene reduction activity

Nitrogenase activity was estimated by measuring acetylene reduction activity (ARA). Fresh roots with attached nodules from five plants were collected together and placed into 20-ml glass vials sealed with rubber septa. Acetylene (1 ml) was injected into the vial and this was incubated at 28°C for 2 h. Finally, a 100-µl gas sample was used to quantify ethylene production using a gas chromatograph (GC-4000A; East & West Analytical Instruments, Beijing, China).

RNA-seq profiling and analysis

For time-course transcriptomic profiling, nodules of MG-20 plants at 4 wpi were harvested daily during 6 d of treatment with 10 mM KNO_3 (T0–T6) and then during 5 d of nitrate removal (R1–R5). Three biological replicates, each consisting of 5–8 nodulated plants, were prepared for the samples at each time point. Total RNA was extracted using a TransZol Plant kit (TransGen Biotech, Beijing, China) based on the manufacturer's protocol and the quality was verified with an Agilent 2100 Bioanalyzer (Agilent Technologies, Santa Clara, CA, USA). RNA libraries were prepared using a NEB Next Ultra II RNA Library Prep Kit (New England Biolabs, Ipswich, MA, USA). Paired-end reads were pre-processed by FASTP (0.22.0) (Chen *et al.*, 2018). High-quality reads were mapped to the *L. japonicus* v.3.0 genome (http://www.kazusa.or.jp/lotus/) using HISAT2 v.2.0.5 (Kim *et al.*, 2019) with default parameters, and BAM files were sorted using SAMTOOLS (1.11) (Li *et al.*, 2009). Aligned reads were assigned to annotated genomic features by FeatureCounts program from RSUBREAD package (1.32.4) (Liao *et al.*, 2019) to generate reads count matrices, and FPKM (fragments per kilobase of transcript per million mapped reads) values representing the expression level were calculated. Transcripts with low reads count across all samples were filtered out using filterByExpr in EDGER with default parameters. Co-expressed transcripts were clustered by their FPKM values using CLUST software (v.1.12.0; Parameter setting: -n 101 3 4, -t 0.7) (Abu-Jamous & Kelly, 2018).

For RNA-seq analysis of NAC-overexpressing (NAC-OE) plants, nodules were harvested at 3 wpi with three biological replicates, each consisting of 5–10 nodulated plants. RNA extraction and raw data processing followed the same procedures as described above. Using the output FPKM values, differentially expressed genes (DEGs) between NAC-OE and GUS-OE samples were identified using EDGER package (3.30.3) (Robinson *et al.*, 2010) with a false discovery rate < 0.05 and |fold change| > 2 as the threshold. Kyoto Encyclopedia of Genes and Genomes (KEGG) pathway information was obtained from KOBAS database (http://kobas.cbi.pku.edu.cn/). KEGG enrichment analysis for each cluster was conducted with the CLUSTERPROFILER package. Transcription factors were annotated based on the TF family information from PLANTTFDB v.5.0 (Tian *et al.*, 2020).

DAP-seq profiling and analysis

Genomic DNA was extracted from mature leaves of MG-20 plants using a MICH DNA Clean Beads (Bluescape Hebei Biotech, Baoding, China) with two biological replicates. The MICH TLX DNA-Seq Kit (Bluescape Hebei Biotech) was used for the library construction. DAP-seq experiments were carried out based on a published protocol (Bartlett *et al.*, 2017). Specifically, the NAC094 protein was prepared using the TNT SP6 Coupled Wheat Germ Extract System (Promega), then immobilized on Magne HaloTag Beads (Promega), and incubated with the constructed DNA library. Unbound DNA fragments were removed by washing the beads three times. The NAC094-binding DNA fragments were then eluted and amplified with indexed primers. Illumina NovaSeq instrument was used for subsequent sequencing (Illumina, San Diego, CA, USA). Reads were mapped to the *L. japonicus* genome v.3.0 using BOWTIE2 (Langmead & Salzberg, 2012). To identify NAC094-binding sites, DAP-seq peaks were screened with MACS2 (Fold enrichment > 2 and q value < 0.05; Zhang *et al.*, 2008). Next, the HOMER software (Heinz *et al.*, 2010) was used for analyzing the localizations of DAP-seq peaks upstream or downstream of the transcription start site within 1-kb region. BEDTOOLS (Quinlan & Hall, 2010) was used to identify the NAC094-targeted genes. Motif identification was performed using the MEME-CHIP suite 5.0.5 (Machanick & Bailey, 2011). NAC094-binding sites and DAP-seq peaks were visualized in INTEGRATIVE GENOMICS VIEWER.

Metabolomics analysis

Nodules from wild-type (WT) MG-20 and *nac094-1* mutant plants were used for metabolomics analysis. Mature nodules at 4 wpi were treated with 10 mM KNO_3 for 1 wk to obtain WT + N and nac + N nodules. Wild-type and *nac094-1* nodules at 5 wpi without nitrate were used as controls (WT and nac). Four types of nodules were used for metabolite extraction, with four biological replicates for each type of nodule. Nodules from 16 plants were collected for each replicate and *c.* 100 mg of nodules were ground in liquid nitrogen. The homogenate was resuspended with prechilled methanol (80%) by vigorous shaking and, after 5 min of incubation on ice, it was centrifuged at 15 000 ***g***, 4°C for 20 min. The supernatant was diluted to a final concentration of 53% methanol with LC–MS grade water and was centrifuged again at 15 000 ***g***, 4°C for 20 min. The final supernatant was injected into the LC–MS/MS system for metabolite identification. LC–MS/MS analyses were performed using an ExionLC™ AD system coupled with a QTRAP® 6500+ mass spectrometer (Sciex, Framingham, MA, USA). Metabolites were annotated using the KEGG database (http://www.genome.jp/kegg/), HMDB database (http://www.hmdb.ca/), and LIPIDMAPS database (http://www.lipidmaps.org/). Metabolites with variable influence on projection (VIP) > 1, *P* value < 0.05, and |fold change| > 2 were identified as differentially accumulated metabolites (DAMs). Principal component analysis and volcano plots were performed using OMICSHARE TOOLS (http://www.omicshare.com/tools). Heatmaps were illustrated with the TBTOOLS and relative metabolite contents shown in the heatmap for four types of nodules were normalized using the zero-to-one method at each column or row scale, setting the maximal value of each metabolite to one (Chen *et al.*, 2020).

Quantitative real-time PCR

Total RNA was isolated from nodules using the TransZol Plant (TransGen Biotech) with three biological replicates. For quantitative real-time PCR (qRT-PCR), complementary DNA was constructed using 1 μg total RNA as input materials following the instructions of the HiScript II Q RT SuperMix kit (Vazyme, Nanjing, China). qRT-PCR was performed using the TransStart Tip Green qPCR SuperMix (TransGen Biotech) on a Real-Time PCR Detection System (CFX384; Bio-Rad). *Ubiquitin* (*Ubq1*, Lj5g3v2060710) and *ATPase* (Lj5g3v2169420) were used as reference genes. Primers used for qRT-PCR are provided in Table S1.

Electrophoretic mobility shift assay

Recombinant MBP-NAC094 protein was expressed and purified from *Escherichia coli*. 6-FAM (6-carboxyfluorescein) was used for labeling DNA fragments. Details are given in Methods S1.

Transactivation assays in *Nicotiana benthamiana*

The corresponding constructs were introduced into *A. tumefaciens* EHA105 and subsequently transformed into *N. benthamiana* leaves (Lasierra & Prat, 2018). The effector constructs (EV, NAC094, NLP1, and NLP4) were paired with the corresponding reporter constructs containing various promoters. The luminescence signal was captured and the LUC : REN ratios were obtained. Detailed procedures are described in Methods S1.

Statistical analysis

All data were analyzed using GraphPad PRISM (9.0.0). For comparison of two groups, two-tailed Student's *t*-test was used as indicated. For comparison of multiple groups, one-way ANOVA analysis and Tukey *post-hoc* tests were used to determine statistical significances as indicated by different letters.

Results

Transcriptomics reveals that an NAC-type TF is involved in nodule senescence

Previous studies have uncovered mechanisms by which nitrate regulates the symbiotic interaction and nodule organogenesis of legumes (Lin *et al.*, 2018, 2021; Nishida *et al.*, 2018, 2021). However, little is known about the molecular mechanism of nitrate-induced premature nodule senescence. We first analyzed the nitrate-triggered phenotypic changes on mature nodules of *L. japonicus* MG-20 at 4 wpi with *M. loti* MAFF303099. Plants were exposed to 10 mM KNO_3 for 7 d. Nodule samples were analyzed daily during nitrate treatment (T0–T7). Nodule color changed from red to green at T5 (Fig. S1a), consistent with the immunoblots showing a substantial decline of Lb content at T5 (Fig. S1b). Although the nitrogenase proteins NifH and NifK were relatively stable during nitrate treatment, ARA of nitrate-treated nodules was dramatically reduced at T3 (Fig. S1c), preceding the Lb degradation and color changes of senescent nodules at T5.

We next performed a time-course transcriptomic study to investigate the genome-wide effects of nitrate on gene expression in nodules. MG-20 nodulated plants at 4 wpi were exposed to 10 mM KNO_3 for 6 d and then nitrate was removed for 5 d (Fig. 1a). Nodule samples were collected daily during nitrate treatment (T0–T6) or nitrate removal (R1–R5). Expression analyses of the mapped 50 526 genes from 12 time-point samples identified two clusters bearing high correlations with nitrate supply and removal (Dataset S1a). Cluster 1 genes (Nitrate-C1; 6051 genes) were initially downregulated by nitrate treatment and then upregulated after nitrate removal (Fig. 1b; Dataset S1b). Cluster 2 genes (Nitrate-C2; 4881 genes) displayed an opposite expression pattern (Fig. 1c; Dataset S1c). Representative genes of these two clusters include an Lb gene (*Lb2*) (Fig. 1d) and a cysteine protease gene (*CYP1*) (Fig. 1e), respectively. KEGG analysis shows that pathways of carbon metabolism and amino acid biosynthesis were enriched in Nitrate-C1, whereas plant–pathogen interaction, autophagy, and signaling responses were enriched in Nitrate-C2 (Fig. S2). Transcriptomic data indicate that nitrate supply to plants resulted in dramatic expression changes of thousands of genes in nodules.

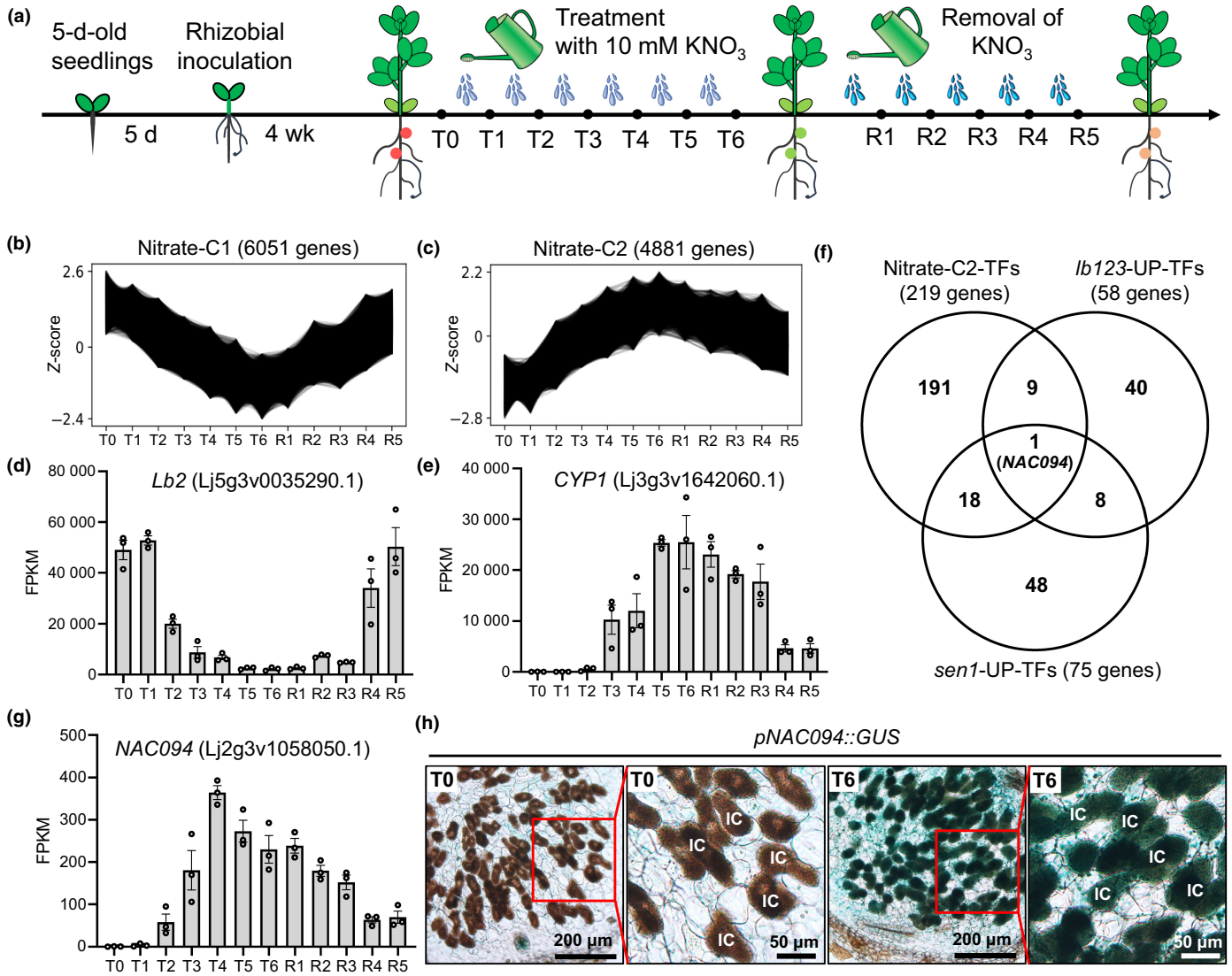

Fig. 1 Transcriptomic analysis of nitrate-responsive genes in mature nodules. (a) Schematic of *Lotus japonicus* nodule sampling during 6 d of 10 mM KNO_3 treatment (T0–T6), followed by 5 d of nitrate removal (R1–R5). (b, c) Two main clusters of differentially expressed genes during nitrate-induced nodule senescence. Biological triplicates, each consisting of 5–8 nodulated plants, were prepared. The expression levels of 6051 genes in Cluster 1 decreased during nitrate treatment and increased after nitrate removal (b), whereas the expression levels of 4881 genes in Cluster 2 showed opposite patterns (c). Each black line shows the expression change of a particular gene during nitrate treatment and removal, represented by the *Z*-score. (d, e) Expression profiles of representative genes of Cluster 1 (*Lb2*) and Cluster 2 (cysteine protease, *CYP1*). FPKM, fragments per kilobase of exon model per million mapped fragments. Data are means ± SE of three biological replicates. (f) Venn diagram showing overlapping of three sets of genes encoding transcription factors (TFs): nitrate-responsive Cluster 2 (Nitrate-C2-TFs), upregulated genes in *lb123* triple mutant nodules (*lb123*-UP-TFs) (Wang *et al*., 2019), and upregulated genes in *sen1* mutant nodules (*sen1*-UP-TFs) (Høgslund *et al*., 2009). (g) Changes in transcript abundance of the unique TF (*NAC094*) during nitrate treatment and removal. (h) Expression of the *pNAC094::GUS* reporter in nodules at 4 wk post-inoculation (wpi) treated with 10 mM KNO_3 for up to 6 d (T0–T6). Enlarged images are displayed on the right side of original images. Images are representative of at least five independent stable transgenic lines. IC, infected cell. (h) Bars: 200 or 50 μm in original or enlarged images, respectively.

To identify key TFs mediating nitrate-induced transcriptional activations, we searched Nitrate-C2 genes and found 219 putative TFs (Nitrate-C2-TFs; Dataset S2a). This dataset was compared to previously identified upregulated TFs in *lb123* or *sen1* mutants (*lb123*-UP-TFs and *sen1*-UP-TFs; Dataset S2b,c), which are two Fix^- mutants that exhibit premature nodule senescence (Høgslund *et al*., 2009; Wang *et al*., 2019). Surprisingly, only one TF (Lj2g3v1058050) was identified in all three datasets (Fig. 1f; Dataset S2d). Indeed, Lj2g3v1058050 was the most upregulated TF in both *lb123* and *sen1* mutant nodules relative to their corresponding WT nodules (Dataset S2b,c). This gene encodes a member of the NAC family of TFs, which we have designated *NAC094* based on its homolog in *A. thaliana*, *ANAC094* (At5g39820) (Fig. S3). The expression pattern of *L. japonicus NAC094* is representative of Nitrate-C2 genes. The transcript abundance of *NAC094* started to increase at T2, peaked at T4, and gradually decreased during nitrate withdrawal (Fig. 1g). Promoter-GUS analysis in stably transformed MG-20 plants showed that the GUS staining signal was dramatically enhanced from T0 to T6 and that most of the signal was

restricted to the infected cells (Fig. 1h). The fluorescence signal of the NAC094-GFP fusion protein was exclusively localized to the nucleus of *N. benthamiana* leaves (Fig. S4). These results hint at a possible role of NAC094 in regulating nitrate-induced nodule senescence in *L. japonicus*.

Ectopic expression of *NAC094* induces premature nodule senescence

To investigate the function of NAC094 *in vivo*, we overexpressed *NAC094* in the infected cells of nodules using an *L. japonicus Lb2* expression cassette (Wang *et al.*, 2019). To this end, we used a *GUS* overexpression construct as a control and analyzed stably transformed plants to detect symbiotic phenotypes. At 4 wpi, *NAC094*-overexpressing plants (NAC-OE1 and NAC-OE2) exhibited a strong SNF deficiency phenotype compared with control plants (GUS-OE). This phenotype included stunted plant growth (Fig. 2a), appearance of white nodules (Fig. 2b), increased nodule numbers (Fig. 2c), reduced shoot biomass (Fig. 2d), and reduced nitrogenase activity (ARA; Fig. 2e). By contrast, under non-symbiotic growth conditions, 1-month-old NAC-OE plants showed similar levels of shoot length and shoot biomass to the GUS-OE control plants (Fig. S5). We next performed toluidine blue staining of nodule sections (Fig. 2f,g) and also examined ultrastructural changes of infected cells by electron microscopy (Fig. 2h,i). The NAC094-OE1 nodules at 2 wpi showed general deterioration of the infected cells, which largely affected symbiosome integrity (Fig. 2f–i). Immunoblots showed an almost complete loss of Lbs and a drastic reduction of the rhizobial proteins NifH and NifK in the two NAC094-OE lines (Fig. 2j). Taken together, these results show that overexpression of *NAC094* causes premature senescence of nodules.

To identify the mechanism by which NAC094 regulates nodule senescence, we performed a transcriptome profiling analysis of nodules at 3 wpi. Around 13 850 DEGs were identified by comparing NAC-OE with control nodules ($|\text{Log}_2\text{FC}| > 1$, FDR < 0.05). Of these, 7516 were upregulated (NAC-OE-UP) and 6334 were downregulated (NAC-OE-DOWN) (Dataset S3a–c). To identify the genes whose expression was affected in both NAC094-OE and WT plants after nitrate treatment, we compared the NAC-OE DEGs with the Nitrate-C1 and Nitrate-C2 clusters. We found that, among the NAC-OE-UP genes, only 142 genes overlapped with Nitrate-C1, whereas 2141 genes overlapped with Nitrate-C2 (Fig. 2k; Dataset S4a). By contrast, among the NAC-OE-DOWN genes, 1957 were common to Nitrate-C1 and only 29 genes overlapped with Nitrate-C2 (Fig. 2l; Dataset S4b). These results indicate that ectopic expression of *NAC094* promotes nodule senescence in the absence of nitrate signal, but also that NAC094-regulated genes largely overlap with nitrate-responsive genes.

NAC094 activates expression of *SAGs* by binding to a conserved sequence motif

To identify binding sites and nodule *SAGs* that are directly targeted by NAC094, we used DAP-seq, which allows the capture of the NAC094 regulatory targets at the whole-genome scale. For this experiment, we used genomic DNA of *L. japonicus* leaves because rhizobial DNA predominates in nodules, which poses a serious technical challenge for the *in vitro* binding of NAC094 to the genomic DNA of nodules. A total of 2819 binding peaks corresponding to 2721 genes were identified from two biological repeats of the DAP-seq experiment (Fig. 3a; Dataset S5). More than 81% of the enriched peaks were localized in promoter (1727) or intergenic (558) regions (Fig. 3b). Analysis of the binding peaks by MEME identified the most enriched motif (Motif 1), with an *E*-value of 1.1e-419, that contains a nearly palindromic 15-bp conserved sequence (5′-DVCGTGDNNDKNACG-3′) (Fig. 3c). Distribution analysis shows that Motif 1 is positioned predominantly at the summit of the NAC094 binding peaks, which indicates that Motif 1 is a highly reliable motif (Fig. 3d). Other two less enriched motifs with larger *E*-values were also identified (Motif 2, 5′-YGCCGT-3′; Motif 3, 5′-CGSCGGYGVMG-3′; Fig. S6a–d). Motif 1, but not Motif 2 or Motif 3, resembles the binding motifs of the *A. thaliana* NAC family of TFs identified in high-throughput DAP-seq studies, including the regulator of leaf senescence, ANAC092 (Fig. S6e; O'Malley *et al.*, 2016). This prompted us to examine the biochemical interactions between NAC094 and gene promoters based on Motif 1.

Differences between nodule and leaf genomic DNAs, such as epigenetic modifications, may influence the results of DAP-seq. To better understand the NAC094-mediated transcriptional regulation in nodules, we compared DAP-seq and nodule RNA-seq data. In the latter case, we included the NAC-OE-UP and Nitrate-C2 genes (Datasets S1c, S3b, S5) and identified a core group of 171 genes that are shared by the three datasets (Fig. 3e; Dataset S6). Three genes were chosen for further analysis, which are functionally uncharacterized and annotated in the Lotus databases as lysozyme (*LYS*), peptide transporter (*PTR*), and copper transporter (*COPT*). Significantly enriched NAC094 binding peaks were identified in the promoter region of these genes in two DAP-seq repeats (Fig. 3f). Electrophoretic mobility shift assay confirmed the *in vitro* binding of NAC094 to corresponding synthetic oligonucleotide probes that contain the core motif in the promoter regions of *LYS*, *PTR*, and *COPT* (Fig. 3g). In addition, we performed a transactivation assay in *N. benthamiana* leaves and consistently observed that NAC094 could activate expression of the firefly luciferase (LUC) reporter driven by the promoters of these three genes (Fig. 3h). Furthermore, promoter deletion analysis was performed to test the requirement of the NAC094 binding region in the transactivation assay (Fig. S7a,b). Around 100-bp deletions abolished the activation of *LYS* and *PTR* promoters by NAC094. However, both WT and truncated *COPT* promoters showed similar level of activation (Fig. S7c,d). The discrepancy could be due to the presence of unidentified NAC094 binding sites outside of the 100-bp deletion fragment.

Cysteine proteases (CYPs) are well-known markers of nodule senescence (Fujie *et al.*, 2009; Yang *et al.*, 2019; Zhou *et al.*, 2021). We observed that a set of *CYPs* were upregulated in NAC-OE nodules and clustered into the Nitrate-C2 dataset, suggesting a role of NAC094 in the transcriptional regulation

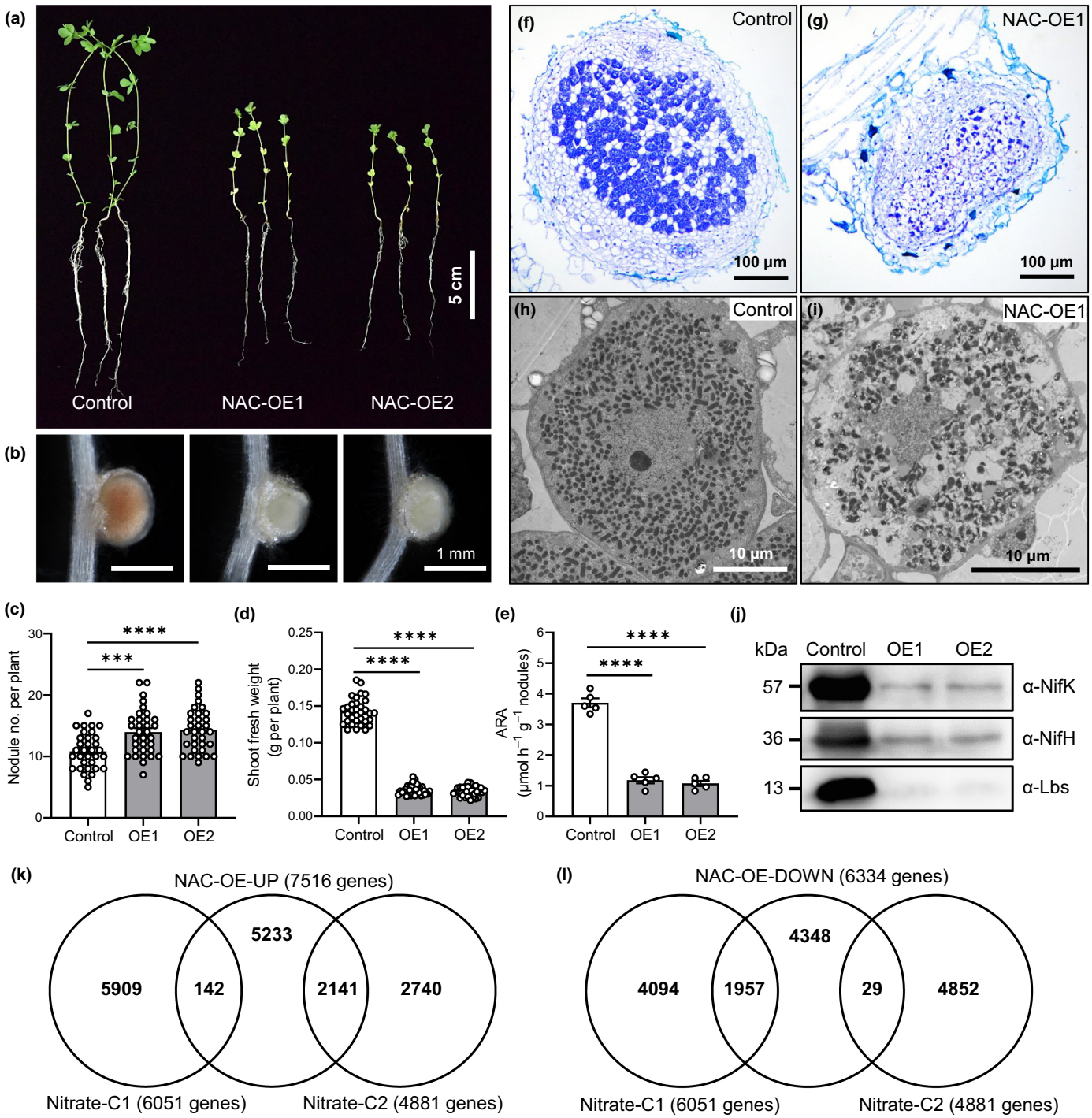

Fig. 2 Nodule senescent phenotype of *NAC094* overexpressing plants. (a–e) Symbiotic phenotypes of *GUS* overexpressing (Control) and *NAC094* overexpressing stable transgenic plants (NAC-OE1, NAC-OE2) at 4 wpi (wk post-inoculation), including (a) whole-plant growth, (b) nodule morphology, (c) nodule numbers, (d) shoot fresh weight, and (e) nitrogenase activity (ARA). Expression of *GUS* and *NAC094* was controlled by the *Lb2* promoter. Values are means ± SE of 33 plants (c, d) or 40–50 plants (e) per genotype. Five biological replicates were performed for the ARA assay and each replicate contained nodules from 8 to 10 plants. Student's *t*-test was used for statistical comparison of OE lines with control plants: ***, $P < 0.001$; ****, $P < 0.0001$. Nine independent transgenic plants overexpressing *NAC094* were obtained with similar phenotypes. For simplicity, in this figure only data of two of them are shown. Bars: (a) 5 cm; (b) 1 mm. (f–i) Toluidine blue staining and transmission electron micrographs of nodule sections from control (f, h) and NAC-OE1 nodules (g, i) at 2 wpi. Similar results were obtained for NAC-OE2 nodules. Bars: (f, g) 100 µm; (h, i) 10 µm. (j) Immunoblots of Lbs and nitrogenase proteins in nodules at 4 wpi. The primary antibodies were raised against *Lotus japonicus* Lb2 and *Mesorhizobium loti* NifH and NifK. The Lb2 antibody recognizes all three Lb proteins. (k, l) Comparative transcriptomic analysis between the NAC-OE (at 3 wpi) and nitrate-responsive genes (Fig. 1b,c) in nodules. For NAC-OE RNA-seq, three biological replicates, each consisting of 5–10 nodulated plants, were prepared. Venn diagram shows the number of shared genes by comparing upregulated (NAC-OE-UP) or downregulated (NAC-OE-DOWN) genes with nitrate-responsive Cluster 1 (Nitrate-C1) and Cluster 2 (Nitrate-C2) genes.

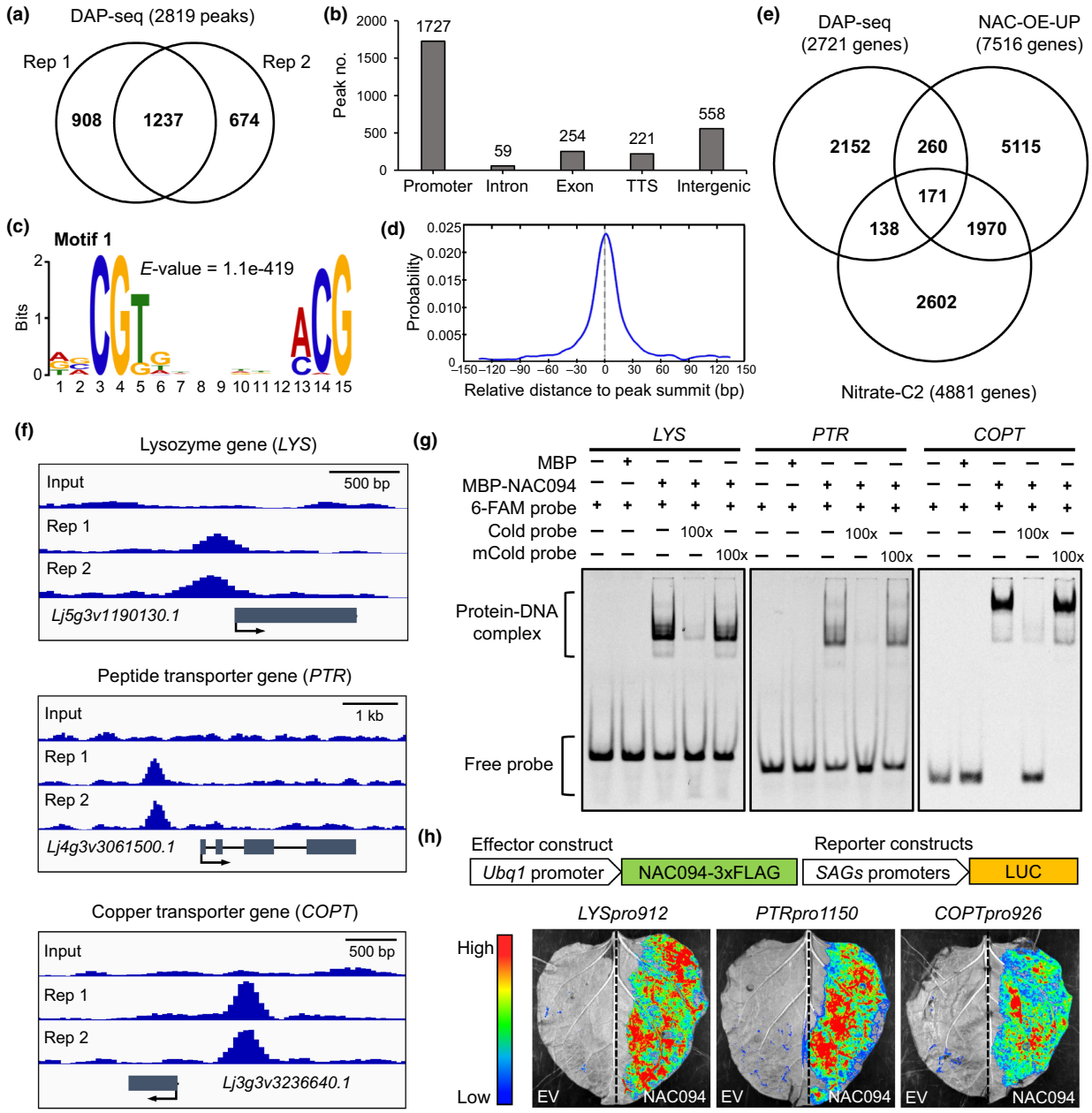

Fig. 3 Identification of NAC094-regulated genes by DNA affinity purification sequencing (DAP-seq). (a) Identification of NAC094 binding sites by DAP-seq. Genomic DNA fragments with manageable sizes (200–400 bp) from *Lotus japonicus* leaves were used for binding with *in vitro* expressed Halo-NAC094 fusion protein. NAC094 binding peaks were identified by comparing the sequencing results between eluates of the binding assay and input of genomic fragments. The Venn diagram indicates the number of overlapping peaks between two biological replicates. (b) Genome-wide distribution of NAC094 binding sites. Promoter, ranging from −2000 to +500 bp relative to the transcription start site (based on MG-20 v.3.0 genome annotation). Transcription termination site (TTS), ranging from −100 to +1000 bp relative to the transcription termination site. (c) Enriched motif within the NAC094 binding peaks. Motif 1 consisting of 15 nucleotides (5′-DVCGTGDNNDKNACG-3′) represents the most significantly enriched core sequence. The *E*-value was calculated by MEME. (d) Centrimo analysis of Motif 1, showing the position of motifs relative to the DAP-seq peak centers. The graph indicates the average density of motif position for all motif-containing regions from position −150 to +150 relative to the DAP-seq peak summit. (e) Venn diagram of overlapping genes in three datasets: DAP-seq, differentially expressed genes upregulated by *NAC094* overexpression (NAC-OE-UP), and nitrate-responsive Cluster 2 genes (Nitrate-C2). (f) Localization of the enriched binding peaks of NAC094 in the promoter regions of representative senescence-associated genes (*SAGs*). The arrow indicates the translation start site and its orientation. 'Input', sequencing results of genomic DNA fragments input as a negative control. (g) Electrophoretic mobility shift assay (EMSA) of the interactions between NAC094 and promoter fragments. Oligonucleotides (42–43 nt) were labeled with 6-FAM. MBP or MBP-NAC094 recombinant proteins were purified from *Escherichia coli* and used for the EMSA assay. An excess of unlabeled oligonucleotides (Cold probe) or mutated oligonucleotides (mCold probe) was used as controls. Probe sequences of *SAGs* were determined according to the location of the binding peaks in DAP-seq results and are listed in Supporting InformationTable S1. (h) Luciferase-activation assay. The signal intensity indicates the levels of NAC094 in activating expression of the firefly luciferase (LUC) reporter driven by the respective *SAG* promoter. EV, empty vector; *Ubq1*, *ubiquitin*. For (g, h), at least three independent experiments were performed and six leaves were used for each experiment. Similar results were observed.

of multiple *CYPs*, including *CYP1* (Lj3g3v1642060), *CYP2* (Lj1g3v4047270), *CYP3* (Lj0g3v0000069), and *CYP4* (Lj1g3v4047250) (Fig. S8a). NAC094 binding peaks were identified only in the promoter region of *CYP1* in the DAP-seq data (Fig. S8b), which may be explained by differences between nodule and leaf genomic DNA materials or by the insufficient coverage of DAP-seq. Indeed, motif prediction analysis using Find Individual Motif Occurrences (Grant *et al.*, 2011) identified sequences related to Motif 1 that are widely present in the promoter regions of *CYP1* and *CYP2/3/4* (Fig. S8c). NAC094 could activate the expression of the luciferase reporter gene driven by the promoters of four *CYP* genes in tobacco leaves (Fig. S8d,e). The transactivation assay was quantified based on the LUC : REN ratio. Promoters of four *CYPs* showed significant activation by NAC094 in heterologous systems (Fig. S8f).

We next analyzed the expression patterns of four *SAGs* by fusing their promoters to the GUS reporter. Results showed that all four promoters were upregulated by nitrate treatment (Fig. S9, compare a and b). The GUS staining signals were mostly concentrated in the infected cells, and weaker signals were observed in the nodule cortical and uninfected cells. These expression patterns were consistent with that of *NAC094* in response to nitrate treatment (Fig. 1h), indicating that NAC094 activates the expression of *SAGs* in the infected cells during nitrate-induced nodule senescence.

Knockout of *NAC094* partially relieves nitrate-induced nodule senescence

To further explore the function of NAC094 in regulating the nitrate response of nodules, we constructed two independent *nac094* null mutants using CRISPR/Cas9 genome editing. Premature stop codons were generated due to the frameshift mutations of exon 2 in both mutants (Fig. 4a). We first compared the phenotype of senescent nodules by treating plants at 4 wpi with 0 or 10 mM KNO_3 for 1 wk. In WT plants, the nodule color changed from pink or red to green after nitrate treatment, whereas the nodules of *nac094-1* and *nac094-2* mutants remained pink or red (Fig. 4b). Immunoblots showed that the nitrogenase proteins NifH and NifK were relatively stable after nitrate supply in the WT and the mutants. However, the Lb content was dramatically reduced in senescent green nodules of WT plants but was much less affected in the mutants (Fig. 4c). Notably, *nac094* mutants showed a substantial decrease (75–85%) in ARA after nitrate supply which was similar to that observed for WT plants (Fig. 4d). We next quantified transcript levels of *Lbs* and four representative NAC094-regulated *SAGs* by qRT-PCR. Upon nitrate supply, *Lb* transcripts were dramatically reduced in both WT and *nac094* nodules (Fig. 4e), which indicates that nitrate-triggered inhibition of *Lb* expression is not mediated by NAC094. Strikingly, the transcriptional activation by nitrate of NAC094-regulated genes (*CYP1*, *LYS*, *PTR*, and *COPT*) was almost completely abolished in *nac094* nodules (Fig. 4f–i). These results convincingly support an essential role of NAC094 in activating expression of a subset of *SAGs* related to nitrate-induced nodule senescence.

NAC094 functions downstream of NLP1 and NLP4 by regulating the expression of *SAGs*

NLP1 and NLP4 were identified as central regulators in controlling multifaceted nitrate effects during legume nodule symbiosis, including the nitrate-induced senescence of mature nodules (Nishida *et al.*, 2018, 2021). We first compared the symbiotic phenotypes of *nlp1*, *nlp4*, and the *nlp1 nlp4* double mutant upon nitrate treatment. Nodulated plants at 4 wpi were treated with 0 or 10 mM KNO_3 for 1 wk. Nodules of WT plants exhibited obvious color changes from red to green with nitrate, whereas the nodules of single or double mutants remained red (Fig. 5a). Immunoblots showed that the Lb content was dramatically reduced in senescent green nodules of WT plants, but was much less affected in the three mutants (Fig. 5b). In addition, WT plants showed a drastic decrease (*c.* 85%) in ARA, whereas the *nlp1* or *nlp4* mutants retained > 50% ARA and the *nlp1 nlp4* mutant was the least affected, with *c.* 80% ARA being retained upon nitrate treatment (Fig. 5c). To investigate the relationship between *NAC094* expression and NLPs during nitrate-induced nodule senescence, we performed qRT-PCR to quantify transcript levels of *Lbs*, *NAC094*, and four NAC094-regulated *SAGs* in the WT and *nlp* mutants. Upon nitrate treatment, *Lb* transcripts were dramatically reduced in WT nodules, whereas various *nlp* mutants retained > 30% of the *Lb* transcript levels (Fig. 5d). Strikingly, the transcriptional activation of *NAC094* and its targeting *SAGs* (*CYP1*, *LYS*, *PTR*, and *COPT*) by nitrate was largely abolished in *nlp* mutant nodules (Fig. 5e–i), except for a little induction of *CYP1* in *nlp4* nodules (Fig. 5f). These results indicate that NLP1 and NLP4 are essential for induction of *NAC094* and that NAC094 functions downstream of NLP1 and NLP4 by regulating the expression of *SAGs* after nitrate supply.

To further dissect the genetic relationship between NAC094 and NLP4 in nitrate-induced nodule senescence, we overexpressed the constitutively active C-terminal region of NLP4 ($NLP4^C$, 544–976 aa) (Nishida *et al.*, 2018, 2021) using the *Lb2* expression cassette in both WT and *nac094-1* plants by hairy root transformation. $NLP4^C$ overexpression (*$NLP4^C$-OE*) resulted in slightly greenish nodules in both genetic backgrounds compared with GUS overexpression (*GUS-OE*), along with decreased red nodule numbers and increased green nodule numbers at 5 wpi (Fig. S10a–c). The transcript level of *NLP4* was doubled in *$NLP4^C$-OE* nodules compared with *GUS-OE* nodules (Fig. S10d). The *Lb* genes were slightly downregulated in *$NLP4^C$-OE* nodules in the two genetic backgrounds (Fig. S10e). In addition, *NAC094* was upregulated in *$NLP4^C$-OE* nodules in WT background (Fig. S10f). Expression of the NAC094-regulated genes was enhanced in *$NLP4^C$-OE*/WT nodules but not in *$NLP4^C$-OE*/*nac094-1* nodules (Fig. S10g–j). These results support again the notion that NAC094 operates downstream of NLP4 by regulating the expression of *SAGs*. Next, we overexpressed *NAC094* in both WT and *nlp4* mutant backgrounds by hairy root transformation. In plants at 5 wpi, *NAC094* overexpression resulted in impaired growth and reduced shoot weight, together with formation of small white/green nodules and

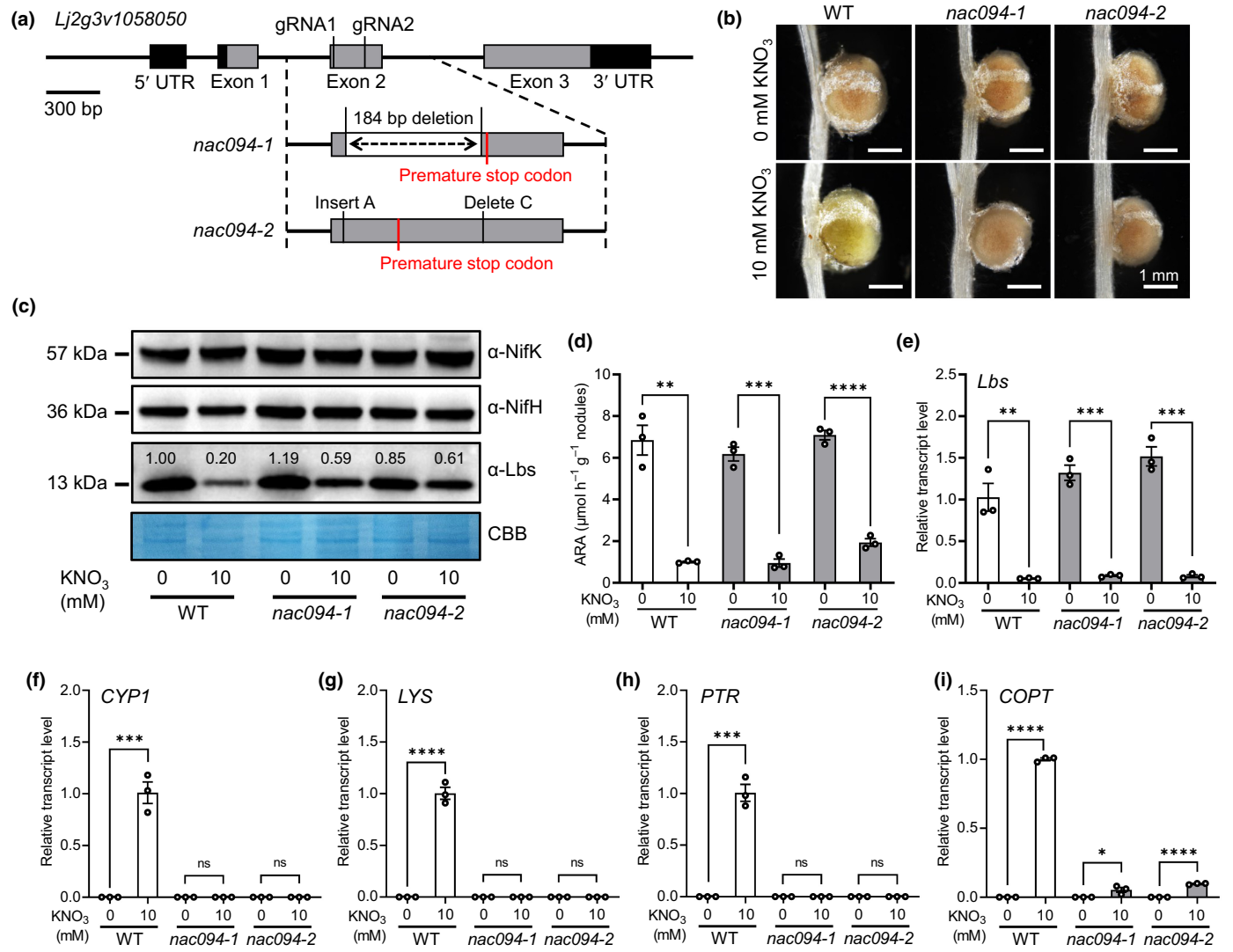

Fig. 4 Characterization of *nac094* null mutants under nitrate treatment. (a) Knockout of *NAC094* by CRISPR-Cas9. The *nac094-1* mutant contains a 184-bp deletion in exon 2. The *nac094-2* mutant has an A insertion and a C deletion. Both mutants contain premature stop codons in exon 2. (b–d) Comparison of symbiotic phenotypes of *nac094* mutants with WT. Plants with mature nodules at 4 wk post-inoculation (wpi) were treated with 10 mM KNO_3 for 1 wk and then (b) nodule morphology, (c) abundance of leghemoglobins (Lbs), NifH and NifK proteins, and (d) acetylene reduction activity were examined. (b) Bars: 1 mm. All immunoblot bands in (c) were obtained from the same PVDF (polyvinylidene difluoride) membrane. Relative band intensities in anti-Lb immunoblots were quantified using ImageJ software. The band intensity of WT nodules at 5 wpi without nitrate treatment was used as control. In (c), Coomassie Brilliant Blue (CBB) staining was used for protein equal loading control. In (d), bars indicate mean values ± SE of three biological replicates. Each replicate contained nodules from five plants. (e–i) qRT-PCR analysis of representative genes including (e) *Lbs* and (f–i) senescence associated genes (*SAGs*). All qRT-PCR data are means ± SE of three biological replicates. Each replicate contained nodules obtained from four plants. Values are normalized against WT plants (e) without nitrate treatment for *Lbs* and (f–i) against WT plants with nitrate treatment for *SAGs*. Student's *t*-test was used for statistical analysis in (d–i) to compare nitrate-treated plants with the untreated plants for each genotype: *, $P < 0.05$; **, $P < 0.01$; ***, $P < 0.001$; ****, $P < 0.0001$; ns, not significant.

decreased red nodule numbers (Fig. S11a–e). These results additionally support that NAC094 acts downstream of NLP4 in activating nodule senescence.

To investigate whether NLP1 or NLP4 could directly activate the expression of *NAC094*, transactivation experiments were performed in tobacco leaves. The promoter of *NITRITE REDUCTASE 1* (*NIR1*, *Lj4g3v0588830.1*), which was shown to be activated by both NLP1 and NLP4 (Nishida *et al.*, 2021; Misawa *et al.*, 2022), was used as a positive control. Results showed that both NLP1 and NLP4 activated the *NIR1* promoter (*c.* 2.6 kb) in tobacco leaves; however, neither of them could enhance the expression of the *NAC094* promoter (*c.* 3.0 kb) (Fig. S12a–e). These results imply that NLP1 and NLP4 could not directly activate the expression of *NAC094* in the heterologous system.

NAC094 regulates metabolic changes during nitrate-induced nodule senescence

To further investigate the function of NAC094 in regulating nitrate-induced nodule senescence, we performed quasi-targeted

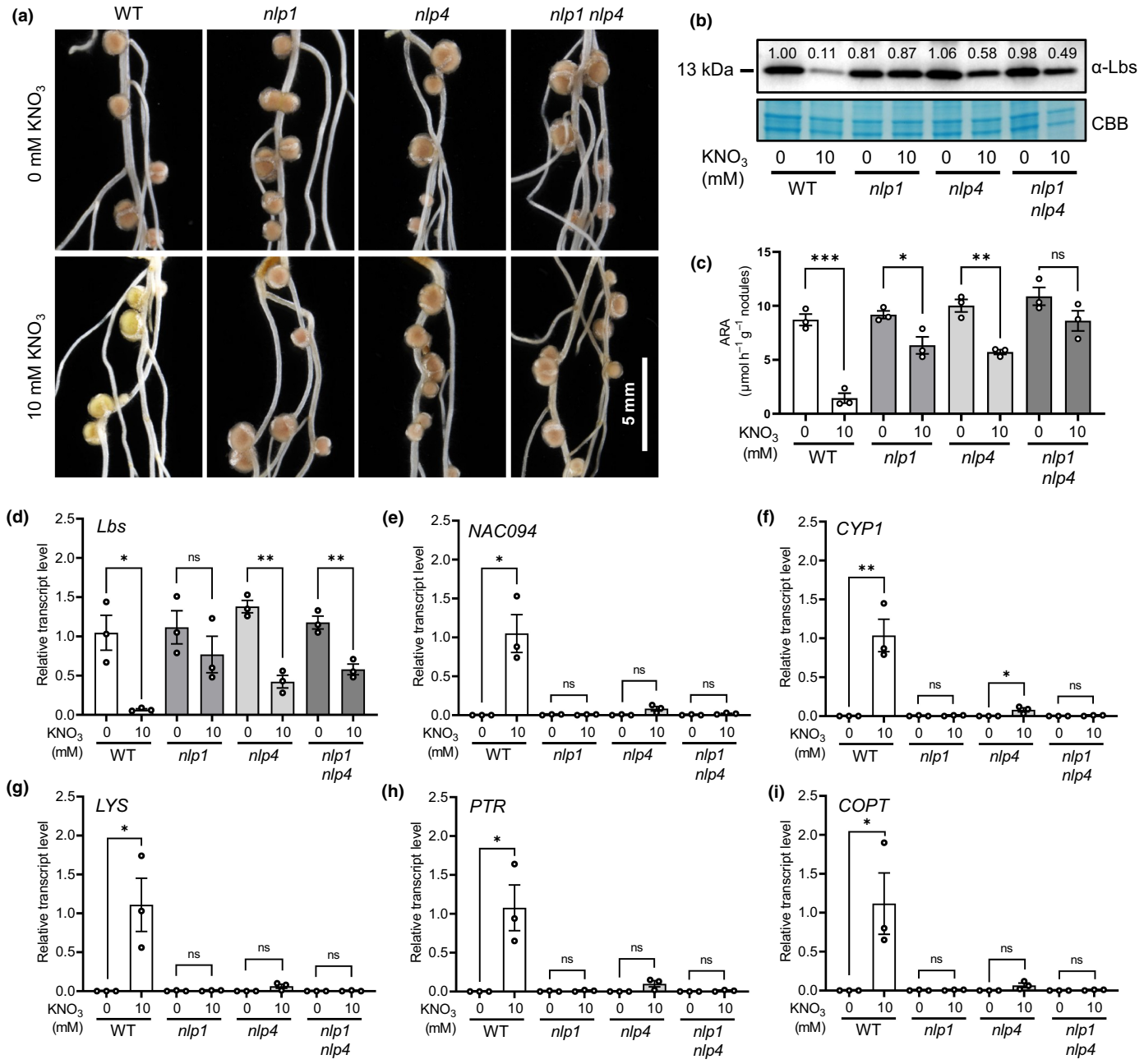

Fig. 5 NLP1 and NLP4 are required for nitrate-induced expression of *NAC094* and senescence-associated genes (*SAGs*). (a–c) Comparison of symbiotic phenotypes of *nlp1*, *nlp4*, and *nlp1 nlp4* mutants with WT. Plants with mature nodules at 4 wk post-inoculation (wpi) were treated with 10 mM KNO_3 for 1 wk and then (a) nodule morphology, (b) abundance of leghemoglobins (Lbs), and (c) nitrogenase activity (ARA) were examined. (a) Bar: 5 mm. Relative band intensities in anti-Lb immunoblots were quantified with ImageJ software. The band intensity of WT nodules at 5 wpi without nitrate treatment was used as control. In (b), Coomassie Brilliant Blue (CBB) staining was used for protein equal loading control. (d–i) qRT-PCR analysis of representative genes including (d) *Lbs*, (e) *NAC094*, and (f–i) *SAGs*. All qRT-PCR data are means ± SE of three biological replicates. Values are normalized against WT plants without nitrate treatment for (d) *Lbs* and (e–i) against WT plants with nitrate treatment for *NAC094* and *SAGs*. Student's *t*-test was used for statistical analysis in (c–i) to compare nitrate-treated plants with the untreated plants for each genotype: *, $P < 0.05$; **, $P < 0.01$; ***, $P < 0.001$; ns, not significant. Bars indicate mean values ± SE. In (c), each replicate contained nodules from five plants. In (d–i), each replicate contained nodules obtained from four plants.

metabolomic analysis and characterized the changes of metabolite concentration in nodules (4 wpi) of WT or *nac094-1* plants treated with 10 mM KNO_3 for 7 d (WT + N or nac + N), or in nodules (5 wpi) of WT or *nac094-1* plants not treated with nitrate (WT or nac) (Fig. 6a). A total of 1038 metabolites were quantified among the four types of nodules (Dataset S7a). Principal component analysis showed that four biological replicates of each type of nodules were clustered together within their respective confidence ellipse ($P < 0.05$). Wild-type and nac nodules exhibited a closer correlation with overlapping confidence ellipse,

New Phytologist

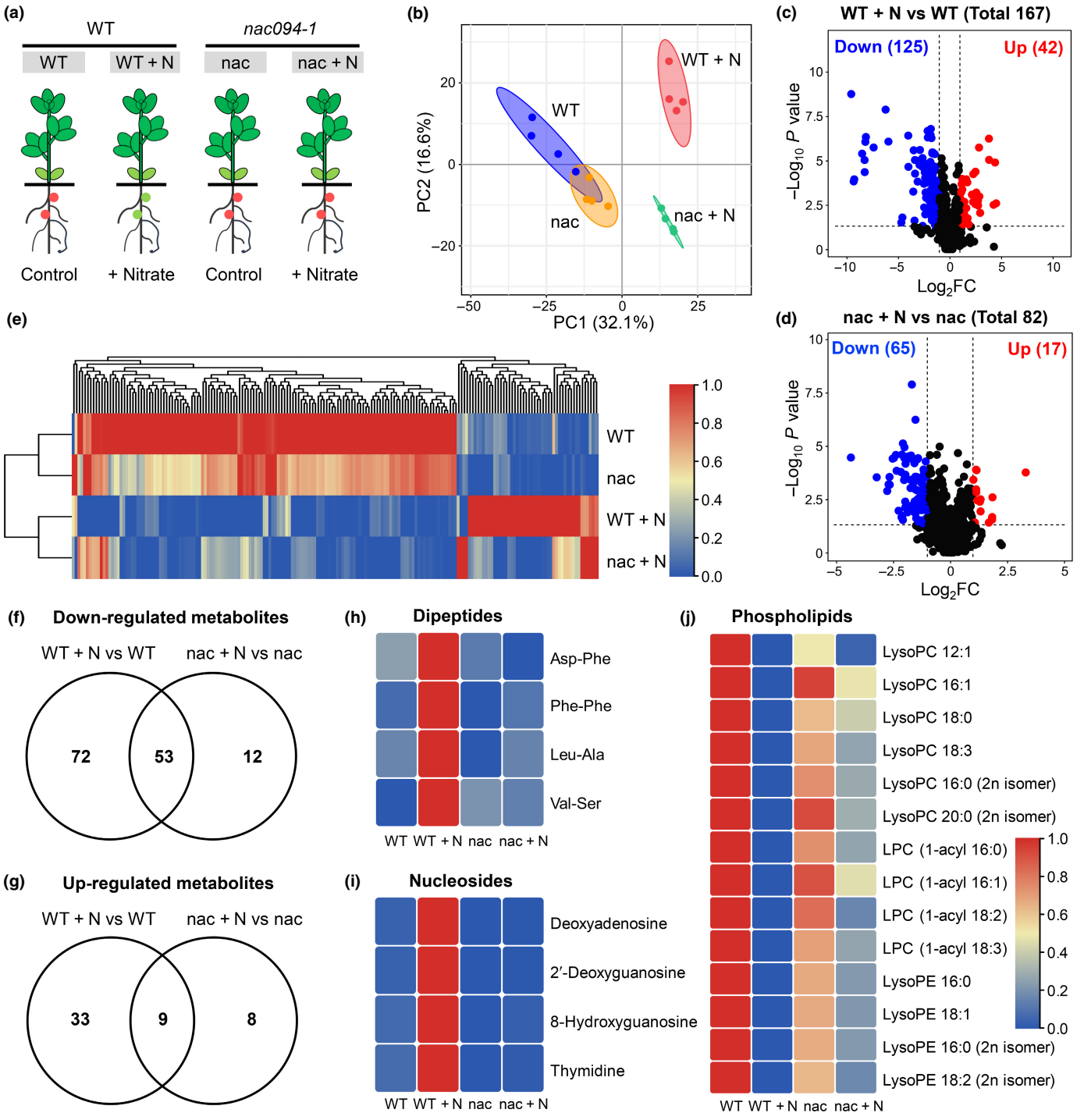

Fig. 6 Metabolomic characterization of *nac094* mutant during nitrate-induced nodule senescence. (a) Diagram of four types of nodule samples used for quasi-targeted metabolomic analysis. Mature nodules of WT and *nac094-1* at 4 wpi (wk post-inoculation) were treated with 10 mM KNO_3 for 1 wk to obtain WT + N and nac + N nodules. Wild-type and *nac094-1* nodules at 5 wpi without nitrate treatment were used as controls (WT and nac). (b) Principal component analysis (PCA) of metabolomic data. Four biological replicates were used for metabolite profiling and each replicate was the pool of nodules from 16 plants. (c, d) Volcano plots showing distribution of metabolites significantly upregulated or downregulated in (c) WT + N or (d) nac + N in comparison to the untreated control nodules of each genotype (lfold changel > 2, $P < 0.05$). (e) Hierarchical cluster heatmap of 187 differentially accumulated metabolites (DAMs) in two comparison groups (WT + N vs WT, nac + N vs nac). Means of four replicates of each type of nodules were used for the heatmap illustration. (f, g) Venn diagrams show the numbers of overlapping or specific DAMs in comparisons of WT + N vs WT and nac + N vs nac. (h–j) Heatmaps show representative DAMs that are specific to WT + N vs WT but absent from nac + N vs nac, including (h) dipeptides, (i) nucleosides, and (j) phospholipids. Means of four replicates of each type of nodules were used for the heatmap illustration. All values of each metabolite in four types of nodules in (e) and (h–j) were normalized using the zero-to-one method with the TBtools software.

whereas WT + N and nac + N nodules exhibited a more distant correlation, suggesting that the absence of NAC094 resulted in dramatic metabolic changes in nitrate-induced senescent nodules (Fig. 6b). We identified 167 and 82 DAMs, respectively, in WT + N vs WT and nac + N vs nac (|fold change| > 2, $P < 0.05$; Fig. 6c,d; Dataset S7b,c). Analyses of the relative contents of 187 DAMs across the four types of nodules indicated that WT + N vs nac + N had much larger differences (85 DAMs) than WT vs nac (6 DAMs) (Fig. 6e; Dataset S7d,e).

We further compared DAMs in the WT and *nac094* background and found that there were 72 downregulated and 33 upregulated metabolites that were unique to WT + N vs WT but that were absent from nac + N vs nac (Fig. 6f,g; Dataset S7f,g). Among the nitrate-responsive metabolites of WT + N vs WT, we observed a large accumulation of four dipeptides and four nucleosides ($\log_2$FC > 1.1 and $\log_2$FC > 2.88, respectively; Fig. 6h,i), the putative protein and nucleic acid degradation products, and a consistent reduction in the amounts of multiple phospholipids ($\log_2$FC < −1.18; Fig. 6j). By contrast, these metabolites showed little or no significant changes in the comparison of nac + N vs nac (Fig. 6h–j). To link these metabolic changes with the expression of genes regulated by NAC094, we found that large numbers of genes encoding for protease and peptidase, nuclease, and phospholipase were upregulated by nitrate treatment and also by *NAC094* overexpression (Fig. S13a–c). The expression patterns of these genes correspond to the metabolic changes of dipeptides, nucleosides, and phospholipids shown in Fig. 6(h–j). Altogether, these results suggest a role of NAC094 in triggering the degradative processes associated to nodule senescence, presumably by activating the expression of *SAGs*.

Discussion

Nitrate inhibits nodule initiation and, depending on concentration and time of exposure, accelerates nodule senescence (Streeter & Wong, 1988; Escuredo *et al.*, 1996; Dupont *et al.*, 2012; Lin *et al.*, 2018). Our study has focused on nitrate-induced nodule senescence. By combining transcriptomic datasets of genes that are upregulated in nodules with nitrate and of genes that are upregulated in nodules of *sen1* and *lb123* mutants, we have identified a unique TF of the NAC family that is closely associated to nodule senescence, and have functionally characterized the gene using overexpressing (NAC-OE) and knockout (*nac094*) lines. We found that NAC-OE nodules show premature senescence in the absence of nitrate (Fig. 2), whereas *nac094* mutants retain a higher content of Lbs than do the WT plants after 1-wk treatment with 10 mM KNO_3 (Fig. 4). In our study, we included various *nlp* mutants (*nlp1*, *nlp4*, *nlp1 nlp4*) for comparison because it has been reported that *L. japonicus* plants deficient in NLP1 or NLP4 also maintain pink nodules in the presence of 10 mM KNO_3 (Nishida *et al.*, 2018, 2021). We could confirm that the *nlp* mutants are partially insensitive to nitrate, having much higher ARA and transcript and protein levels of Lbs than the WT plants upon nitrate supply (Fig. 5). By contrast, the *nac094* mutants showed a drastic reduction in ARA and *Lb* transcripts which was similar to that of the WT (Fig. 4d,e). Also, the induction of *SAGs* in the mutants was virtually suppressed (Fig. 4f–i). From these data, we conclude that NLP1 and NLP4 are master regulators of the pleiotropic nitrate responses, whereas NAC094 plays a role only in the nitrate-induced senescence of mature nodules by activating the expression of specific genes.

The absence of NLP1 or NLP4 attenuated the upregulation of *NAC094* and NAC094-targeted *SAGs* in nitrate-treated nodules (Fig. 5e–i). Correspondingly, the upregulation of *NAC094* and *SAGs* in $NLP4^C$-OE nodules in the WT background was found to be inhibited in the *nac094* mutant (Fig. S10f–j). In addition, *NAC094* overexpression triggered premature nodule senescence in both the WT and *nlp4* mutant (Fig. S11). In the presence of nitrate, NLP4 translocates from the cytoplasm to the nucleus (Nishida *et al.*, 2018), whereas NAC094 was consistently localized to the nuclei (Fig. S4). These results support the hypothesis that NAC094 functions downstream of NLP1 and NLP4 (Fig. 7). However, the NLP4 binding site was not identified in the promoter region of *NAC094* based on DAP-seq analysis (Nishida *et al.*, 2021). In this study, both NLP1 and NLP4 failed to enhance the expression of the LUC reporter driven by a *c.* 3-kb promoter fragment of *NAC094* which shows auto-activation in tobacco leaves (Fig. S12). *Arabidopsis thaliana* NLP7 was identified as a nitrate sensor by direct interaction with nitrate (Liu *et al.*, 2022), implying that a similar mechanism may exist for *L. japonicus* NLP1, NLP4, or other NLP protein(s). Because the transcript abundance of *NAC094* was highly upregulated by nitrate treatment, we propose that other signaling components (for example, additional TFs) downstream of NLP1/4 are responsible for activating *NAC094* expression (Fig. 7).

Color changes from pink or red to green is a typical feature of senescing nodules, which is largely caused by the breakdown of Lbs (Dupont *et al.*, 2012). Previous studies showed that green pigments in senescent nodules could be Lbs with modified heme (Navascués *et al.*, 2012) or heme degradation products (Virtanen & Laine, 1946). In this study, changes in pink to green color were highly correlated with decreased Lb contents in nitrate-induced senescent nodules. Notably, we found that NAC094 activates the expression of multiple *CYP* genes (Fig. S8). These genes encode cysteine proteases with a purported function in the degradation of Lbs and other nodule proteins (Fujie *et al.*, 2009; Yang *et al.*, 2019). Cysteine proteases with acidic pH optima (5.0–5.5) are especially active in degrading Lbs and the intracellular pH becomes acidic in senescing nodules (Pladys *et al.*, 1988; Pladys & Vance, 1993). Therefore, the lack of activation of *CYP1* with nitrate in the *nac094* mutants is consistent with the maintenance of substantial Lb protein levels in nodules, and the same may be the case of the *nlp* mutants (Figs 4, 5). The color change was also observed in nodules showing $NLP4^C$ overexpression in *nac094* background, even though the induction of *CYP1* was almost blocked by the absence of NAC094 (Fig. S10). These results indicate that multiple Lb degradation pathways, such as autophagy and other proteolytic phenomena, might be present in different types of nodule senescence (Vauclare *et al.*, 2010; Yang *et al.*, 2019). Notably, there is an apparent inconsistency between the absence of Lb transcripts and the

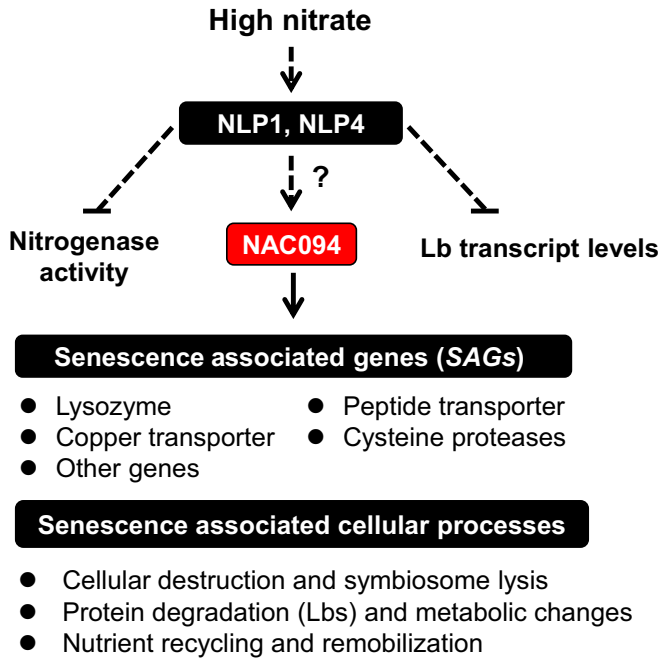

Fig. 7 Model for the role of NAC094 in nitrate-induced nodule senescence. Legume nodule senescence occurs after exposure of plants to high nitrate. NAC094 is a transcriptional regulator whose expression is activated during nitrate-induced nodule senescence. NLP1 and NLP4 play essential roles in the nitrate-triggered inhibition of SNF efficiency in mature nodules, including the inhibition of nitrogenase activity and downregulation of leghemoglobin genes (*Lbs*) (indicated with blunt-ended arrows). NLP1 and NLP4 also mediate the nitrate-induced expression of NAC094, although the mechanism is unknown yet (indicated with a question mark). NAC094 functions downstream of NLP1/NLP4 by specifically activating the nitrate-responsive senescence associated genes (*SAGs*). These include the genes encoding lysozyme (LYS), peptide transporter (PTR), copper transporter (COPT), and cysteine proteases (CYPs). Protein products of *SAGs* may play important roles during nodule senescence in processes such as organelle disruption, degradation of Lbs and other important proteins, metabolite alterations, and nutrient recycling and remobilization. Direct and indirect regulatory relationships are indicated by solid and dotted lines, respectively.

presence of Lb proteins in nodules of *nac094* mutants (Fig. 4c,e). This observation does suggest that NAC094 is not involved in the transcriptional regulation of *Lb* genes but in affecting protein stability by regulating *CYP* expression, as already mentioned.

Leaf and nodule senescence are two comparable biological processes that share responsive genes encoding enzymes involved in the degradation of organelles and macromolecules as well as in nutrient remobilization (Van de Velde *et al.*, 2006; De Michele *et al.*, 2009). The degradation of chloroplast, chlorophyll, and chlorophyll-binding proteins in senescent leaves functionally corresponds to the degradation of symbiosome, heme, and heme-binding proteins (mostly Lbs) in senescent nodules, for example, multiple protease genes were actively expressed in senescent leaves and nodules (Yang *et al.*, 2019; Guo *et al.*, 2021; Zhou *et al.*, 2021). The mechanism of leaf senescence has been intensively studied, in sharp contrast to the poorly investigated nodule senescence. ANAC092 (also termed ORE1; At5g39610) is a master regulator that controls leaf senescence, which is induced by multiple endogenous and environmental cues, including aging, darkness, and salinity. ANAC092 directly activates the expression of genes involved in chlorophyll catabolism, nucleic acid degradation, ethylene biosynthesis, and nutrient transport (Woo *et al.*, 2019; Guo *et al.*, 2021). Phylogenetic analysis indicates that ANAC092 and the negative regulator of nodule senescence, MtNAC969, are located in two related branches distant from the LjNAC094 branch (Fig. S3). LjNAC094 is closely related to both ANAC094 and ANAC009. However, ANAC009 is involved in promoting root cap-forming divisions (Willemsen *et al.*, 2008; Bennett *et al.*, 2014) and has a closer homolog in *L. japonicus* (Lj2g3v1278970.1), whereas ANAC094 has been reported but not functionally characterized (Ooka *et al.*, 2003). Based on these analyses, we decided to use the name LjNAC094 for Lj2g3v1058050.1. The evolution of *LjNAC094* and the coevolution with its targeting *SAGs* in *L. japonicus* and other legumes remain an interesting topic for further investigation.

Our study uncovers the key function of NAC094 in nitrate-induced nodule senescence by activating a set of *SAGs* (Figs 4, 5). Besides *CYP1*, *LYS* is a *SAG* with a potential role in decomposition of the bacteroid cell (Liu *et al.*, 2014), whereas *PTR* and *COPT* encode putative membrane transporters (Li *et al.*, 2020). These direct targets of NAC094 encode proteins that have potential functions in degradation of cellular components (CYP1 and LYS) and remobilization of nutrients (PTR and COPT). The involvement of NAC094 in *SAG* regulation is consistent with changes in key metabolites, such as dipeptides, nucleosides, and phospholipids, that we have detected in *nac094* nodules (Figs 6, S8, S13; Dataset S7). Interestingly, the conserved 15-bp binding motif of NAC094 resembles that of ANAC092 (Fig. S6e; O'Malley *et al.*, 2016). These results suggest that NAC094, like ANAC092, is mainly involved in the regulation of catabolic processes and in nutrient recycling during nodule senescence. Moreover, the expression of *NAC094* was induced in nitrate-treated nodules or in the premature senescence of Fix^- nodules (Fig. 1f; Dataset S2). *NAC094* overexpression by itself triggered premature nodule senescence in the absence of nitrate (Figs 2, S11). It would be interesting to investigate whether the module 'NAC094-SAGs' is involved in other types of nodule senescence, such as aging and dark-stress induced senescence.

In summary, NAC094 is a newly identified important regulator that functions downstream of NLP1 and NLP4 to activate a specific group of *SAGs* for the execution of nitrate-induced nodule senescence. These findings open new avenues to investigate the signal transduction pathways of nodule senescence. Our study also provides a new potential strategy to alleviate nitrate inhibition on SNF using mutants less sensitive to nitrate, such as *nac094* together with *nlp1 nlp4* mutants, or mutants of genes involved in nitrate transport and metabolism.

Acknowledgements

We thank Dr Takuya Suzaki (University of Tsukuba, Japan) for providing the *nlp1*, *nlp4*, and *nlp1 nlp4* mutant seeds. This work was supported by the National Natural Science Foundation of China (32000192, 31870220), the Foundation of Hubei

Hongshan Laboratory (2022hszd014), Fundamental Research Funds for the Central Universities (2662020SKPY007), and MCIN/AEI/10.13039/501100011033 (grant PID2020-113985GB-I00). We also thank the BaiChuan fellowship of College of Life Science and Technology, Huazhong Agricultural University, for funding support.

Competing interests

None declared.

Author contributions

LW and DD designed the research. LW, TT, JL, YQ, YZ, and QF performed the experiments. XX, RL, and GN performed the bioinformatics analysis. LW, MB, and DD wrote and revised the manuscript.

ORCID

Manuel Becana https://orcid.org/0000-0002-1083-0804
Deqiang Duanmu https://orcid.org/0000-0002-9365-362X
Guogui Ning https://orcid.org/0000-0001-8891-5229
Longlong Wang https://orcid.org/0000-0003-0537-2711
Xian Xin https://orcid.org/0000-0003-1460-5978

Data availability

Transcriptomic data and DAP-seq data were deposited in Gene Expression Omnibus (GEO) under accession nos. GSE197362, GSE197361, and GSE197359. Sequence data from this article can be found in the Kazusa DNA Research Institute (http://www.kazusa.or.jp/lotus/) and PHYTOZOME (https://phytozome-next.jgi.doe.gov/) under the following accession nos.: *LjNAC094* (Lj2g3v1058050.1), *LjNLP1* (Lj1g3v2295200.1), *LjNLP4* (Lj5g3v1999250.2), *LjLb1* (Lj5g3v0035290.2), *LjLb2* (Lj5g3v0035290.1), *LjLb3* (Lj5g3v0465970.1), *LjCYP1* (Lj3g3v1642060.1), *LjCYP2* (Lj1g3v4047270.1), *LjCYP3* (Lj0g3v0000069.1), *LjCYP4* (Lj1g3v4047250.1), *LjLYS* (Lj5g3v1190130.1), *LjPTR* (Lj4g3v3061500.1), *LjCOPT* (Lj3g3v3236640.1), *LjUbq1* (Lj5g3v2060710.1), *LjATPase* (Lj5g3v2169420.1), *LjNIR1* (Lj4g3v0588830.1), *MtNAC969* (Medtr4g081870.1), *ANAC009* (AT1G26870.1), *ANAC092* (AT5G39610.1), *ANAC094* (AT5G39820.1).

References

Abu-Jamous B, Kelly S. 2018. CLUST: automatic extraction of optimal co-expressed gene clusters from gene expression data. *Genome Biology* **19**: 172.

Bartlett A, O'Malley RC, Huang SSC, Galli M, Nery JR, Gallavotti A, Ecker JR. 2017. Mapping genome-wide transcription-factor binding sites using DAP-seq. *Nature Protocols* **12**: 1659–1672.

Bennett T, van den Toorn A, Willemsen V, Scheres B. 2014. Precise control of plant stem cell activity through parallel regulatory inputs. *Development* **141**: 4055–4064.

Cabeza R, Koester B, Liese R, Lingner A, Baumgarten V, Dirks J, Salinas-Riester G, Pommerenke C, Dittert K, Schulze J. 2014. An RNA sequencing transcriptome analysis reveals novel insights into molecular aspects of the nitrate impact on the nodule activity of *Medicago truncatula*. *Plant Physiology* **164**: 400–411.

Chen C, Chen H, Zhang Y, Thomas HR, Frank MH, He Y, Xia R. 2020. TBTOOLS: an integrative toolkit developed for interactive analyses of big biological data. *Molecular Plant* **13**: 1194–1202.

Chen S, Zhou Y, Chen Y, Gu J. 2018. FASTP: an ultra-fast all-in-one FASTQ preprocessor. *Bioinformatics* **34**: i884–i890.

De Michele R, Formentin E, Todesco M, Toppo S, Carimi F, Zottini M, Barizza E, Ferrarini A, Delledonne M, Fontana P *et al.* 2009. Transcriptome analysis of *Medicago truncatula* leaf senescence: similarities and differences in metabolic and transcriptional regulations as compared with Arabidopsis, nodule senescence and nitric oxide signalling. *New Phytologist* **181**: 563–575.

Deng J, Zhu F, Liu J, Zhao Y, Wen J, Wang T, Dong J. 2019. Transcription factor bHLH2 represses *CYSTEINE PROTEASE77* to negatively regulate nodule senescence. *Plant Physiology* **181**: 1683–1703.

Díaz CL, Grønlund M, Schlaman HRM, Spaink HP. 2005. Induction of hairy roots for symbiotic gene expression studies. In: Márguez AJ, ed. Lotus japonicus *handbook*. Dordrecht, the Netherlands: Springer, 261–277.

Dupont L, Alloing G, Pierre O, El Msehli S, Hopkins J, Herouart D, Frendo P. 2012. The legume root nodule: from symbiotic nitrogen fixation to senescence. In: Nagata T, ed. *Senescence*. Rijeka, Croatia: InTech, 137–168.

Escuredo PR, Minchin FR, Gogorcena Y, Iturbe-Ormaetxe I, Klucas RV, Becana M. 1996. Involvement of activated oxygen in nitrate-induced senescence of pea root nodules. *Plant Physiology* **110**: 1187–1195.

Fujie M, Shintaku H, Maeno H, Kajihara R, Usami S, Yamada T. 2009. Molecular cytological analysis of cysteine proteinases from nodules of *Lotus japonicus*. *Cytologia* **74**: 343–354.

Ge M, Wang Y, Liu Y, Jiang L, He B, Ning L, Du H, Lv Y, Zhou L, Lin F *et al.* 2020. The NIN-like protein 5 (ZmNLP5) transcription factor is involved in modulating the nitrogen response in maize. *The Plant Journal* **102**: 353–368.

Gogorcena Y, Gordon AJ, Escuredo P, Minchin FR, Witty JF, Moran JF, Becana M. 1997. Nitrogen fixation, carbon metabolism, and oxidative damage in nodules of dark-stressed common bean plants. *Plant Physiology* **113**: 1193–1201.

Grant CE, Bailey TL, Noble WS. 2011. FIMO: scanning for occurrences of a given motif. *Bioinformatics* **27**: 1017–1018.

Guo Y, Ren G, Zhang K, Li Z, Miao Y, Guo H. 2021. Leaf senescence: progression, regulation, and application. *Molecular Horticulture* **1**: 5.

Heinz S, Benner C, Spann N, Bertolino E, Lin YC, Laslo P, Cheng JX, Murre C, Singh H, Glass CK. 2010. Simple combinations of lineage-determining transcription factors prime *cis*-regulatory elements required for macrophage and B cell identities. *Molecular Cell* **38**: 576–589.

Høgslund N, Radutoiu S, Krusell L, Voroshilova V, Hannah MA, Goffard N, Sánchez DH, Lippold F, Ott T, Sato S *et al.* 2009. Dissection of symbiosis and organ development by integrated transcriptome analysis of *Lotus japonicus* mutant and wild-type plants. *PLoS ONE* **4**: e6556.

Jiang S, Jardinaud MF, Gao J, Pecrix Y, Wen J, Mysore K, Xu P, Sánchez-Cañizares C, Ruan Y, Li Q *et al.* 2021. NIN-like protein transcription factors regulate leghemoglobin genes in legume nodules. *Science* **374**: 625–628.

Kim D, Paggi JM, Park C, Bennett C, Salzberg SL. 2019. Graph-based genome alignment and genotyping with HISAT2 and HISAT-GENOTYPE. *Nature Biotechnology* **37**: 907–915.

Konishi M, Okitsu T, Yanagisawa S. 2021. Nitrate-responsive NIN-like protein transcription factors perform unique and redundant roles in Arabidopsis. *Journal of Experimental Botany* **72**: 5735–5750.

Langmead B, Salzberg SL. 2012. Fast gapped-read alignment with BOWTIE 2. *Nature Methods* **9**: 357–359.

Lasierra P, Prat S. 2018. Transient transactivation studies in *Nicotiana benthamiana* leaves. *Methods in Molecular Biology* **1794**: 311–322.

Li H, Handsaker B, Wysoker A, Fennell T, Ruan J, Homer N, Marth G, Abecasis G, Durbin R, 1000 Genome Project Data Processing Subgroup. 2009. The sequence alignment/map format and SAMTOOLS. *Bioinformatics* **25**: 2078–2079.

Li H, Jiang F, Wu P, Wang K, Cao Y. 2020. A high-quality genome sequence of model legume *Lotus japonicus* (MG-20) provides insights into the evolution of root nodule symbiosis. *Genes* **11**: 483.

Liao Y, Smyth GK, Shi W. 2019. The R package RSUBREAD is easier, faster, cheaper and better for alignment and quantification of RNA sequencing reads. *Nucleic Acids Research* **47**: e47.

Lin J, Roswanjaya YP, Kohlen W, Stougaard J, Reid D. 2021. Nitrate restricts nodule organogenesis through inhibition of cytokinin biosynthesis in *Lotus japonicus*. *Nature Communications* **12**: 6544.

Lin JS, Li X, Luo Z, Mysore KS, Wen J, Xie F. 2018. NIN interacts with NLPs to mediate nitrate inhibition of nodulation in *Medicago truncatula*. *Nature Plants* **4**: 942–952.

Liu KH, Liu M, Lin Z, Wang ZF, Chen B, Liu C, Guo A, Konishi M, Yanagisawa S, Wagner G *et al.* 2022. NIN-like protein 7 transcription factor is a plant nitrate sensor. *Science* **377**: 1419–1425.

Liu KH, Niu Y, Konishi M, Wu Y, Du H, Sun Chung H, Li L, Boudsocq M, McCormack M, Maekawa S *et al.* 2017. Discovery of nitrate-CPK-NLP signalling in central nutrient-growth networks. *Nature* **545**: 311–316.

Liu X, Grabherr HM, Willmann R, Kolb D, Brunner F, Bertsche U, Kühner D, Franz-Wachtel M, Amin B, Felix G *et al.* 2014. Host-induced bacterial cell wall decomposition mediates pattern-triggered immunity in Arabidopsis. *eLife* **3**: e01990.

Loscos J, Matamoros MA, Becana M. 2008. Ascorbate and homoglutathione metabolism in common bean nodules under stress conditions and during natural senescence. *Plant Physiology* **146**: 1282–1292.

Luo Z, Wang J, Li F, Lu Y, Fang Z, Fu M, Mysore KS, Wen J, Gong J, Murray JD *et al.* 2023. The small peptide CEP1 and the NIN-like protein NLP1 regulate *NRT2.1* to mediate root nodule formation across nitrate concentrations. *Plant Cell* **35**: 776–794.

Machanick P, Bailey TL. 2011. MEME-CHIP: motif analysis of large DNA datasets. *Bioinformatics* **27**: 1696–1697.

Minchin FR, Becana M, Sprent JI. 1989. Short-term inhibition of legume N_2 fixation by nitrate: II. Nitrate effects on nodule oxygen diffusion. *Planta* **180**: 46–52.

Misawa F, Ito M, Nosaki S, Nishida H, Watanabe M, Suzuki T, Miura K, Kawaguchi M, Suzaki T. 2022. Nitrate transport via NRT2.1 mediates NIN-LIKE PROTEIN-dependent suppression of root nodulation in *Lotus japonicus*. *Plant Cell* **34**: 1844–1862.

Navascués J, Pérez-Rontomé C, Gay M, Marcos M, Yang F, Walker FA, Desbois A, Abián J, Becana M. 2012. Leghemoglobin green derivatives with nitrated hemes evidence production of highly reactive nitrogen species during aging of legume nodules. *Proceedings of the National Academy of Sciences, USA* **109**: 2660–2665.

Nishida H, Nosaki S, Suzuki T, Ito M, Miyakawa T, Nomoto M, Tada Y, Miura K, Tanokura M, Kawaguchi M *et al.* 2021. Different DNA-binding specificities of NLP and NIN transcription factors underlie nitrate-induced control of root nodulation. *Plant Cell* **33**: 2340–2359.

Nishida H, Suzaki T. 2018. Nitrate-mediated control of root nodule symbiosis. *Current Opinion in Plant Biology* **44**: 129–136.

Nishida H, Tanaka S, Handa Y, Ito M, Sakamoto Y, Matsunaga S, Betsuyaku S, Miura K, Soyano T, Kawaguchi M *et al.* 2018. A NIN-LIKE PROTEIN mediates nitrate-induced control of root nodule symbiosis in *Lotus japonicus*. *Nature Communications* **9**: 499.

O'Malley RC, Huang SSC, Song L, Lewsey MG, Bartlett A, Nery JR, Galli M, Gallavotti A, Ecker JR. 2016. Cistrome and epicistrome features shape the regulatory DNA landscape. *Cell* **165**: 1280–1292.

Ooka H, Satoh K, Doi K, Nagata T, Otomo Y, Murakami K, Matsubara K, Osato N, Kawai J, Carninci P *et al.* 2003. Comprehensive analysis of NAC family genes in *Oryza sativa* and *Arabidopsis thaliana*. *DNA Research* **10**: 239–247.

Pérez Guerra JC, Coussens G, De Keyser A, De Rycke R, De Bodt S, Van De Velde W, Goormachtig S, Holsters M. 2010. Comparison of developmental and stress-induced nodule senescence in *Medicago truncatula*. *Plant Physiology* **152**: 1574–1584.

Pladys D, Barthe P, Rigaud J. 1988. Changes in intracellular pH in French-bean nodules induced by senescence and nitrate treatment. *Plant Science* **56**: 99–106.

Pladys D, Vance CP. 1993. Proteolysis during development and senescence of effective and plant gene-controlled ineffective alfalfa nodules. *Plant Physiology* **103**: 379–384.

Puppo A, Groten K, Bastian F, Carzaniga R, Soussi M, Lucas MM, de Felipe MR, Harrison J, Vanacker H, Foyer CH. 2005. Legume nodule senescence: roles for redox and hormone signalling in the orchestration of the natural aging process. *New Phytologist* **165**: 683–701.

Quinlan AR, Hall IM. 2010. BEDTOOLS: a flexible suite of utilities for comparing genomic features. *Bioinformatics* **26**: 841–842.

Robinson MD, McCarthy DJ, Smyth GK. 2010. EDGER: a BIOCONDUCTOR package for differential expression analysis of digital gene expression data. *Bioinformatics* **26**: 139–140.

Sańko-Sawczenko I, Łotocka B, Mielecki J, Rekosz-Burlaga H, Czarnocka W. 2019. Transcriptomic changes in *Medicago truncatula* and *Lotus japonicus* root nodules during drought stress. *International Journal of Molecular Sciences* **20**: 1204.

Schauser L, Handberg K, Sandal N, Stiller J, Thykjaer T, Pajuelo E, Nielsen A, Stougaard J. 1998. Symbiotic mutants deficient in nodule establishment identified after T-DNA transformation of *Lotus japonicus*. *Molecular and General Genetics* **259**: 414–423.

Streeter J, Wong PP. 1988. Inhibition of legume nodule formation and N_2 fixation by nitrate. *Critical Reviews in Plant Sciences* **7**: 1–23.

Suganuma N, Nakamura Y, Yamamoto M, Ohta T, Koiwa H, Akao S, Kawaguchi M. 2003. The *Lotus japonicus Sen1* gene controls rhizobial differentiation into nitrogen-fixing bacteroids in nodules. *Molecular Genetics and Genomics* **269**: 312–320.

Tian F, Yang DC, Meng YQ, Jin JP, Gao G. 2020. PLANTREGMAP: charting functional regulatory maps in plants. *Nucleic Acids Research* **48**: D1104–D1113.

Tirichine L, Herrera-Cervera JA, Stougaard J. 2005. Transformation-regeneration procedure for *Lotus japonicus*. In: Márquez AJ, ed. Lotus japonicus *handbook*. Dordrecht, the Netherlands: Springer, 279–284.

Van de Velde W, Guerra JC, De Keyser A, De Rycke R, Rombauts S, Maunoury N, Mergaert P, Kondorosi E, Holsters M, Goormachtig S. 2006. Aging in legume symbiosis. A molecular view on nodule senescence in *Medicago truncatula*. *Plant Physiology* **141**: 711–720.

Vauclare P, Bligny R, Gout E, De Meuron V, Widmer F. 2010. Metabolic and structural rearrangement during dark-induced autophagy in soybean (*Glycine max* L.) nodules: an electron microscopy and ^{31}P and ^{13}C nuclear magnetic resonance study. *Planta* **231**: 1495–1504.

Vidal EA, Alvarez JM, Araus V, Riveras E, Brooks MD, Krouk G, Ruffel S, Lejay L, Crawford NM, Coruzzi GM *et al.* 2020. Nitrate in 2020: thirty years from transport to signaling networks. *Plant Cell* **32**: 2094–2119.

Virtanen AI, Laine T. 1946. Red, brown and green pigments in leguminous root nodules. *Nature* **157**: 25–26.

Wang L, Rubio MC, Xin X, Zhang B, Fan Q, Wang Q, Ning G, Becana M, Duanmu D. 2019. CRISPR/Cas9 knockout of leghemoglobin genes in *Lotus japonicus* uncovers their synergistic roles in symbiotic nitrogen fixation. *New Phytologist* **224**: 818–832.

Wang L, Wang L, Tan Q, Fan Q, Zhu H, Hong Z, Zhang Z, Duanmu D. 2016. Efficient inactivation of symbiotic nitrogen fixation related genes in *Lotus japonicus* using CRISPR-Cas9. *Frontiers in Plant Science* **7**: 1333.

Wang YY, Cheng YH, Chen KE, Tsay YF. 2018. Nitrate transport, signaling, and use efficiency. *Annual Review of Plant Biology* **69**: 85–122.

Willemsen V, Bauch M, Bennett T, Campilho A, Wolkenfelt H, Xu J, Haseloff J, Scheres B. 2008. The NAC domain transcription factors FEZ and SOMBRERO control the orientation of cell division plane in Arabidopsis root stem cells. *Developmental Cell* **15**: 913–922.

Woo HR, Kim HJ, Lim PO, Nam HG. 2019. Leaf senescence: systems and dynamics aspects. *Annual Review of Plant Biology* **70**: 347–376.

Wu J, Zhang ZS, Xia JQ, Alfatih A, Song Y, Huang YJ, Wan GY, Sun LQ, Tang H, Liu Y *et al.* 2020. Rice NIN-LIKE PROTEIN 4 plays a pivotal role in nitrogen use efficiency. *Plant Biotechnology Journal* **19**: 448–461.

Yang L, Syska C, Garcia I, Frendo P, Boncompagni E. 2019. Involvement of proteases during nodule senescence in leguminous plants. In: de Bruijn F, ed. *The model legume* Medicago truncatula. Hoboken, NJ, USA: John Wiley & Sons, 683–693.

Yu J, Xuan W, Tian Y, Fan L, Sun J, Tang W, Chen G, Wang B, Liu Y, Wu W *et al.* 2021. Enhanced OsNLP4-OsNiR cascade confers nitrogen use efficiency by promoting tiller number in rice. *Plant Biotechnology Journal* **19**: 167–176.

de Zélicourt A, Diet A, Marion J, Laffont C, Ariel F, Moison M, Zahaf O, Crespi M, Gruber V, Frugier F. 2012. Dual involvement of a *Medicago truncatula* NAC transcription factor in root abiotic stress response and symbiotic nodule senescence. *The Plant Journal* **70**: 220–230.

Zhang W, Willows RD, Deng R, Li Z, Li M, Wang Y, Guo Y, Shi W, Fan Q, Martin SS *et al.* 2021. Bilin-dependent regulation of chlorophyll biosynthesis by GUN4. *Proceedings of the National Academy of Sciences, USA* **118**: e2104443118.

Zhang Y, Liu T, Meyer CA, Eeckhoute J, Johnson DS, Bernstein BE, Nusbaum C, Myers RM, Brown M, Li W *et al.* 2008. Model-based analysis of ChIP-Seq (MACS). *Genome Biology* **9**: R137.

Zhou S, Zhang C, Huang Y, Chen H, Yuan S, Zhou X. 2021. Characteristics and research progress of legume nodule senescence. *Plants* **10**: 1103.

Supporting Information

Additional Supporting Information may be found online in the Supporting Information section at the end of the article.

Dataset S1 RNA-seq profiling of nitrate-responsive genes in MG-20 nodules.

Dataset S2 Comparison of upregulated transcription factors in datasets of senescent nodules.

Dataset S3 RNA-seq profiling of differentially expressed genes in NAC094-overexpressing nodules.

Dataset S4 Comparison of conserved differentially expressed genes between NAC-OE and nitrate-responsive transcriptomes.

Dataset S5 Enriched peaks in DAP-seq global profiling of NAC094 binding sites.

Dataset S6 Conserved and NAC094-regulated genes (171 genes) in DAP-seq, NAC-OE-UP, and Nitrate-C2 datasets.

Dataset S7 Metabolomic analysis of wild-type and *nac094-1* mutant nodules at 4-wpi with or without 10 mM KNO_3 treatment.

Fig. S1 Characterization of wild-type (MG-20) nodules under nitrate treatment.

Fig. S2 Gene enrichment analysis of Nitrate-C1 and Nitrate-C2 clusters.

Fig. S3 Phylogenetic analysis of *Lotus japonicus* NAC094 homologous proteins.

Fig. S4 Subcellular localization of LjNAC094 in *Nicotiana benthamiana* leaves.

Fig. S5 Phenotypic analysis of NAC094-OE plants under non-symbiotic growth conditions.

Fig. S6 Two less enriched binding motifs of LjNAC094 and comparison of LjNAC094- and ANAC092-binding motifs.

Fig. S7 Promoter deletion analysis of senescence-associated genes in transactivation assay.

Fig. S8 NAC094 activates the promoters of four cysteine protease genes in *Nicotiana benthamiana* leaves.

Fig. S9 Expression pattern of four senescence-associated genes under nitrate treatment.

Fig. S10 NAC094 is required for induction of senescence-associated genes caused by $NLP4^{C}$ overexpression.

Fig. S11 *NAC094* overexpression induces premature nodule senescence in both the wild-type and *nlp4* mutant.

Fig. S12 Transactivation assay of NLP1 and NLP4 in regulating *NAC094* expression.

Fig. S13 Expression patterns of NAC094-regulated genes related to protein, nucleic acid, and phospholipid degradation.

Methods S1 Supplemental materials and methods describing plant growth and transformation, plasmid constructs, plant transformation, GUS staining, protein subcellular localization, immunoblot analysis, transmission electron microscopy, electrophoretic mobility shift assay, transactivation assays, and phylogenetic analysis.

Table S1 Primers and probes used in this study.

Please note: Wiley is not responsible for the content or functionality of any Supporting Information supplied by the authors. Any queries (other than missing material) should be directed to the *New Phytologist* Central Office.